Photoluminescence and X-ray Diffraction Analyses of Cadmium Zinc Telluride Crystals

by

Ramin Jamnejad
B.Sc. , University of Tehran , 2007

A Thesis Submitted in Partial Fulfillment
of the Requirements for the Degree of

MASTER OF APPLIED SCIENCE

in the Department of Electrical and Computer Engineering

Supervisory Committee

Photoluminescence and X-ray Diffraction Analyses of Cadmium Zinc Telluride Crystals

by

Ramin Jamnejad
B.Sc. , University of Tehran , 2007

Supervisory Committee

Dr. Thomas Tiedje, Department of Electrical and Computer Engineering
Supervisor

Dr. Reuven Gordon, Department of Electrical and Computer Engineering
Departmental Member

Abstract

Supervisory Committee
Dr. Thomas Tiedje, Department of Electrical and Computer Engineering
Supervisor
Dr. Reuven Gordon, Department of Electrical and Computer Engineering
Departmental Member

This thesis present photoluminescence spectroscopy and X-ray diffraction analyses of four different cadmium zinc telluride samples with different quality and features and similar zinc molar concentration of 10%.

Photoluminescence spectroscopy of the samples let us obtain several physical parameters of the samples which are indicators of quality, composition, structure, and impurity levels of the samples. The band gap energy of the samples obtained from the photoluminescence spectra at low temperatures helped us to estimate zinc molar concentration of the samples. Temperature dependence of band gap energy in these samples has been analyzed and exciton-LO phonon interactions in the samples has been analyzed. From temperature dependence of full width at half maximum of the photoluminescence peak several parameters including concentration of impurity centers and inhomogeneity of the samples are determined and compared in order to check the quality of the samples. Thermal quenching of the photoluminescence peak has been analyzed and the processes which are associated with each parameter are determined and discussed.

X-ray diffraction analyses of the sample for the location and width of the peaks have been analyzed and several characteristics of the samples including quality, lattice constant and zinc molar concentration of the samples are determined and compared. The parameters that are obtained from these analyses are compared with the ones from the photoluminescence spectra and showed a good agreement between the results of these two non-destructive characterization techniques.

Table of Contents

List of Tables

List of Figures

Acknowledgments

Foremost, I would like to express my sincere gratitude to my supervisor Dr. Thomas Tiedje for his continuous support and guidance during my research. His patience, motivation, and knowledge always helped me to overcome any challenges that I faced during this work and without his helps, this work would be impossible to be done for me. I am very grateful for the opportunity that was given to me to work under supervision of him.

Beside my supervisor, I would like to thank the company that supported this research study, RedLen. I would like to specially thank Dr. Henry Chen, Saeid Taherion, Leon Gusak and Georgios Prekas from RedLen for their help and guidance during my work on this project.

Furthermore, I would like to express my gratitude to the rest of my committee members, Dr. Reuven Gordon and Dr. Sadik Dost, for the interest they showed to my research and their support throughout my work.

I feel blessed to be able to work with friendly and knowledgeable colleagues and friends in Molecular Epitaxy Laboratory at University of Victoria, Ryan, Mostafa and Vahid. Their presence, support and the extended talks that we had together about our researches, helped me significantly, and for that, I very grateful.

Dedication

To Ana, my best motive and support

and

My family without whom this work could not have been done

1 Introduction

The general topic of this thesis is about cadmium zinc telluride crystals and its applications in radiation detectors and medical imaging systems. In this chapter, a general introduction to cadmium zinc telluride is presented. Then, the organization of this thesis is explained.

Cadmium Zinc Telluride: An Introduction

Cadmium zinc telluride ($Cd_{1-x}Zn_xTe$) is a ternary II-VI compound that has been used in many nuclear detector applications these days as it shows several favorable features such as optical band gap, and ability to work at room temperature. Since 1970s, silicon and germanium X-ray detectors doped with lithium are being used in X-ray medical imaging systems that require liquid nitrogen cooling systems to operate. As CZT X-ray detectors work at room temperature and do not require expensive cooling solutions, they provide a cost-efficient alternative for the conventional semiconductor X-ray detectors. Furthermore, it contains relatively heavy elements that give it a high stopping power for medical X-rays. Added to all of these features are the convenient electrical properties such as high resistivity and charge transport that make CZT-based detectors able to operate at a high performance level. In addition to these applications, CZT is the substrate of choice for growing high quality and homogenous crystals of mercury cadmium telluride ($Hg_{1-y}Cd_yTe$) which is used for infrared detection. Using CZT as the substrate reduces the stress during the growth and improves the crystal quality significantly. To match the lattice spacing of these two compounds in order to grow dislocation-free

HgCdTe on top of CZT, different concentrations of zinc should be used for each percentage of cadmium in mercury cadmium telluride crystal.

A lot of research interest is shown in CZT growth and device fabrication in order to meet growing demand for CZT radiation detectors for medical and non-medical purposes. CZT detectors especially draw a lot of attention for room-temperature x-ray and gamma ray detectors. [1], [2]

We can categorize radiation into two separate groups, the ones that are charged, such as beta particles consisting of electrons and positrons, and alpha particles and the ones that are not charged, such as x-rays and gamma rays. Relaxation of an excited nucleus to low energy states and destruction of electrons and positrons can emit a gamma ray photon. X-rays can be produced when a fast moving electron interacts with its surroundings and emits photons. The main difference between these radiations is the energy of the emitted photon. For example, X-ray photons have energies in the range from 1 keV to 100 keV, while gamma ray photons have energies greater than 100 keV. When CZT crystals are hit by a gamma ray, an electric signal can be measured across the two faces of the crystal. The strength of this signal depends on the quality of the CZT crystal. The reader should note that detection of this radiation was only possible by using expensive systems which operate at cryogenic temperatures, while CZT detectors operate at room temperature, which reduces the cost of the system.

The efficiency of a CZT detector depends on two major factors: the general quality of the bulk crystal and the surface quality. These factors affect several aspects of radiation detection such as charge collection efficiency, radiation stopping power, and

homogeneity of the whole detector. Growing large CZT single crystals with acceptable quality to be used in detectors is a challenging task as CZT has relatively low thermal conductivity compared to other semiconductors and it hinders controlling the solid liquid interface which is mainly controlled by melting-point isotherm that is controlled by the heat transfer during the growth[3]. Maintaining a planar solid liquid interface during the growth is one of the main necessities to grow large high quality single crystal bulks[4]. High ionicity of the CZT structure facilitates the formation of defects inside the crystal during the growth process, as higher ionicities result in lower formation energies for dislocations and stacking faults[5]. A new method of crystal growth has been introduced for CZT by Zanio[6] called asymmetrical Bridgman method. The main feature of this method is maintaining a planar solid liquid interface during the growth process. Sen et al.[7] used this method to grow CZT crystals with diameters as large as 5 cm and resistivity as high as 10^{11} Ω-cm.

Other than the quality of the crystal which includes density of dislocations, stacking faults, impurities, antisites and vacancies in the crystal, the band gap of the semiconductor plays a major role in the operation of a detector. The bandgap of CZT crystals can be adjusted by changing the zinc concentration in the alloy, from 1.5 eV for CdTe to 2.3 eV for ZnTe[8], [9]. Higher band gaps help to reduce the leakage current noise in the detectors and allow the detector to work at higher temperatures with lower noise levels. However, too large of a band gap requires more energy to produce electron hole pairs in the semiconductor and a higher probability of carriers being trapped, which decreases the efficiency of the detector. Adjusting the trade-off between a low band gap

energy for lower electron hole pair activation energy and lower trapping probability and a higher band gap energy for lower noise levels and the ability to work at higher temperatures gives an optimal range for the band gap between 1.5 eV to 2.2 eV which is perfectly aligned with the band gap in CZT crystals.

Semiconductor radiation detectors in general are fabricated from semiconductors such as germanium, silicon, cadmium telluride, mercuric iodide, and CZT. Silicon detectors only present acceptable resolution in detecting radiation with energies less than a few tens of kilo electron volts, while the detector itself can work at room temperature[10]. On the other hand, high purity germanium (HPGe) detectors exhibit an extremely high resolution which is a result of its high number of charge carriers due to its low band gap of less than 1 eV[11]. However, having low band gap energy causes a high level of thermal noise at high temperatures and makes it necessary to operate the detector at cryogenic temperatures. High atomic number semiconductor materials such as CdTe, HgI, and CZT are recently being used in radiation detectors for operation at room temperature with relatively high efficiency. Among these, lower production costs and the adjustable band gap energy of CZT make this particular crystal stand out.

Organization of Thesis

This thesis focuses on the theory and application of cadmium zinc telluride crystals in radiation detectors and medical imaging systems. A comprehensive non-destructive method for determination of the quality of CdZnTe crystals is studied and results are discussed.

In chapter 2, a review of theories behind photoluminescence and X-ray diffraction, as main focuses of this work, is provided.

In chapter 3, experimental methods used during this thesis work are explained.

In chapter 4, the results and performed analyses on these data are presented and results of these analyses are discussed.

In chapter 5, a conclusion for this thesis and a summary of the work that has been done is presented.

2 Theory

In this chapter, a general description of the theory behind photoluminescence and X-ray diffraction is reviewed. These two experimental techniques are the focus of this work.

Photoluminescence

Photoluminescence can provide useful information about a semiconductor material, its structure, composition and quality. Several localized energy levels are typically present in the band gap, both shallow and deep levels. Shallow levels have small energy differences with the top of the valance band or bottom of the conduction band, while deep levels are more widely separated in energy from the band edges. Radiative recombination of charge carriers only happens when the carriers are transferred to the conduction or valance band. No charge carrier can get radiatively recombined while it is trapped in a localized energy level in the band gap. Transfer of the charge carrier to the conduction or valance band can occur by different stimulation processes such as an electric field, light exposure, or thermal excitation. When a pre-excited material shows a luminescence effect after being heated, this is the release of the preciously stored energy from the electromagnetic radiation, and it is called thermo-luminescence. The presence of vacant lattice sites, impurities or any other kind of defect can provide trapping centers for the charge carriers, which facilitate non-radiative recombination and reduces radiative recombination.

Photoluminescence occurs in solid materials when electron states of the solid are excited by light and the excitation energy gets released through a recombination process

and the emission of a photon. Stoke's rule[12] is the first law that governs this process and according to it the radiated photon always has an energy equal to or less than the excitation energy. In other words, the radiated photon always has wavelengths equal or longer than the excitation photon. The difference between these two levels is due to non-radiative energy transfers in the solid. P. J. Dean[13] published a general introduction to photoluminescence spectroscopy.

In general, the process of a photoluminescence spectroscopy starts with exposing the surface of the probed material with a monochromic light beam with a photon energy higher than the band gap. The absorbed photon creates an electron hole pair and they move to states in the conduction band or within the gap. These excited carriers can transfer to lower energy levels within the gap or the valence band and emit the stored energy in the form of a photon. These radiated photons then get collected and studied for the purpose of spectroscopy. These photons carry the energy signature of different levels available in the material due to impurities, defects, and the material structure. Studying these photons then provides a comprehensive overview of the point defects in the material and the specific type of each present defect, impurity or structural feature. Usually the photons that are emitted in the recombination process involve conduction band to valence band transitions, are not present in the photoluminescence spectra, as some of these photons get reabsorbed in the material. Only photons with energies lower than the band gap are able to escape the crystal and be observed in the photoluminescence spectra.

As Coulomb's law indicates, any pair of objects carrying opposite electric charge will attract to each other by a Coulomb force. In the case of a free electron in the conduction band and a free hole in the valence band, the Coulomb interaction of these charge carriers binds them weakly together. This entity composed of a weakly bond free electron-free hole pair is called an exciton. Excitons can be regarded as a mobile energy packet and when they are not trapped by any defect or impurity, its energy can be expressed by a hydrogen model as:

$$E_X = E_g - \frac{2\pi^2 m_r^* q^4}{h^2 \varepsilon^2}$$

where E_g is the band gap energy, h is Plank's constant, ε is the dielectric constant and m_r^* is the reduced effective mass of the pair described as:

$$\frac{1}{m_r^*} = \frac{1}{m_e^*} + \frac{1}{m_h^*}$$

where m_e^* and m_h^* is the electron and hole effective masses respectively.

Inclusion of zinc in cadmium telluride crystals changes the band gap and free exciton energy. Hence these energies depends on zinc molar concentration x in $Cd_{1-x}Zn_xTe$. We assumed that the free exciton energy varies almost linearly from 10 meV in CdTe to 13 meV in ZnTe and it is assumed to be 10.8 meV[14] for the materials in our study for which x~9%. The dependence of band gap energy on zinc molar concentration is discussed in detail in chapter 4.

Interaction of free excitons with defect centers or impurities changes the total energy of the combination. Whenever the interaction reduces the energy, the exciton will be trapped on the defect or impurity and it is regarded as a bound exciton. These bound excitons can

participate in a radiative recombination process from which photons with energies lower than free exciton related photons are emitted. These photons appear as a peak in the photoluminescence spectra at an energy level lower than the peak for free excitons.

Both neutral and ionized donor and acceptor atoms can trap a free exciton. In general, four types of bound excitons are usually detectable: excitons bound to ionized donors (D^+,X), excitons bound to neutral donors (D^0,X), excitons bound to ionized acceptors (A^-,X), and excitons bound to neutral acceptors (A^0,X)[15], [16].

All of these bound exciton types have been reported in photoluminescence spectra of CZT except the ionized acceptor (A^-,X). Several published articles[17], [18] investigated the appearance of these bound exciton peaks in different materials and it is reported that free excitons can bind to an ionized donor when the ratio of the mass of holes to the mass of electrons is higher than 1.4 and to an ionized acceptor when the ratio of the mass of electrons to the mass of holes is higher than 1.4[17], [18]. Therefore, it is not possible to see both (D^+,X) and (A^-,X) peak in one material. As for CZT the mass of holes is about three times the mass of electrons, therefore only (D^+,X) peak can be detected.

Different energy levels present in CZT are shown in figure 2.1[19]. In addition to levels shown in this figure, a free exciton level with an energy of 10.8 meV less than the conduction band, a donor-bound exciton level with an energy of around 12-14 meV less than the bandgap, and an acceptor-bound exciton level with energy of around 160-170 meV less than the bandgap is present in CZT.

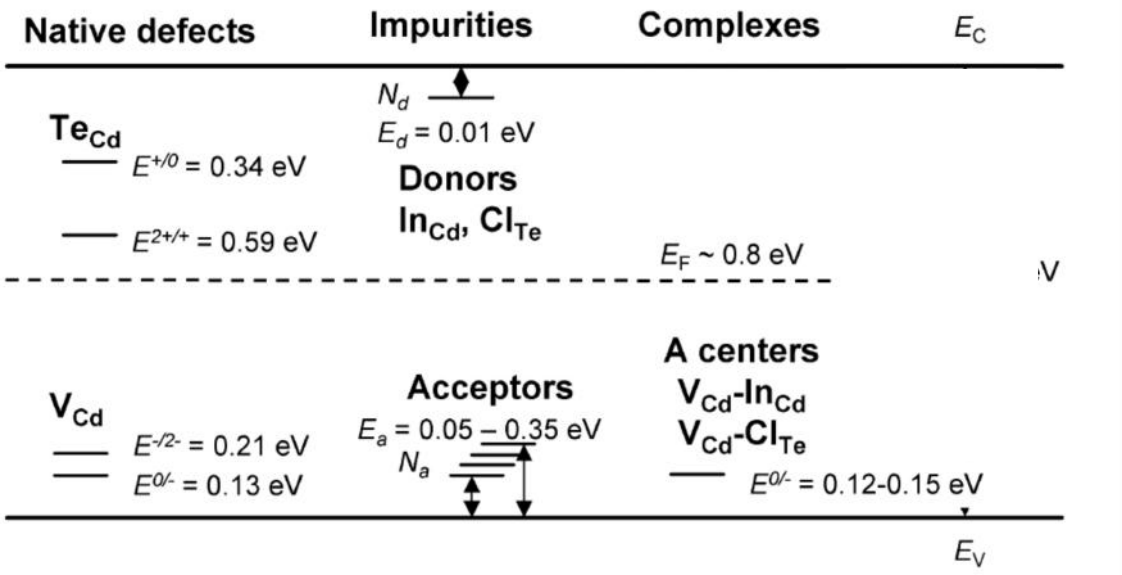

Figure 2.1 Position of energy levels in CZT

CZT crystals usually contain both donor and acceptor atoms and they are referred as n-type or p-type according to which type of dopant is dominant. These donor and acceptors can form an interacting pair with each other and the Coulomb energy between them will change the binding energies of the isolated impurities. The energy of the photon resulting from a recombination of an electron on a donor and hole on an acceptor is described as:

$$E_{photon} = E_g - (E_A + E_D) + \frac{e^2}{\varepsilon R}$$

where E_g is the band gap energy, E_A and E_D are acceptor and donor ionization energies respectively, e is electron charge, ε is the dielectric constant and R is the distance between donor and acceptor atoms. This emission results in a wide peak due to a range of donor-acceptor separations in the photoluminescence spectra that is usually detectable in CZT. A vacancy of cadmium in CZT and CdTe can be included in this band while behaving as an acceptor. In CdTe a wide peak in range of 1.4 eV to 1.5 eV is visible due

to DAP recombination. For CZT crystals with low zinc molar concentration, the same feature is expected as well.

A diagram of several recombination processes that can be detected in CZT is shown in figure 2.2[20].

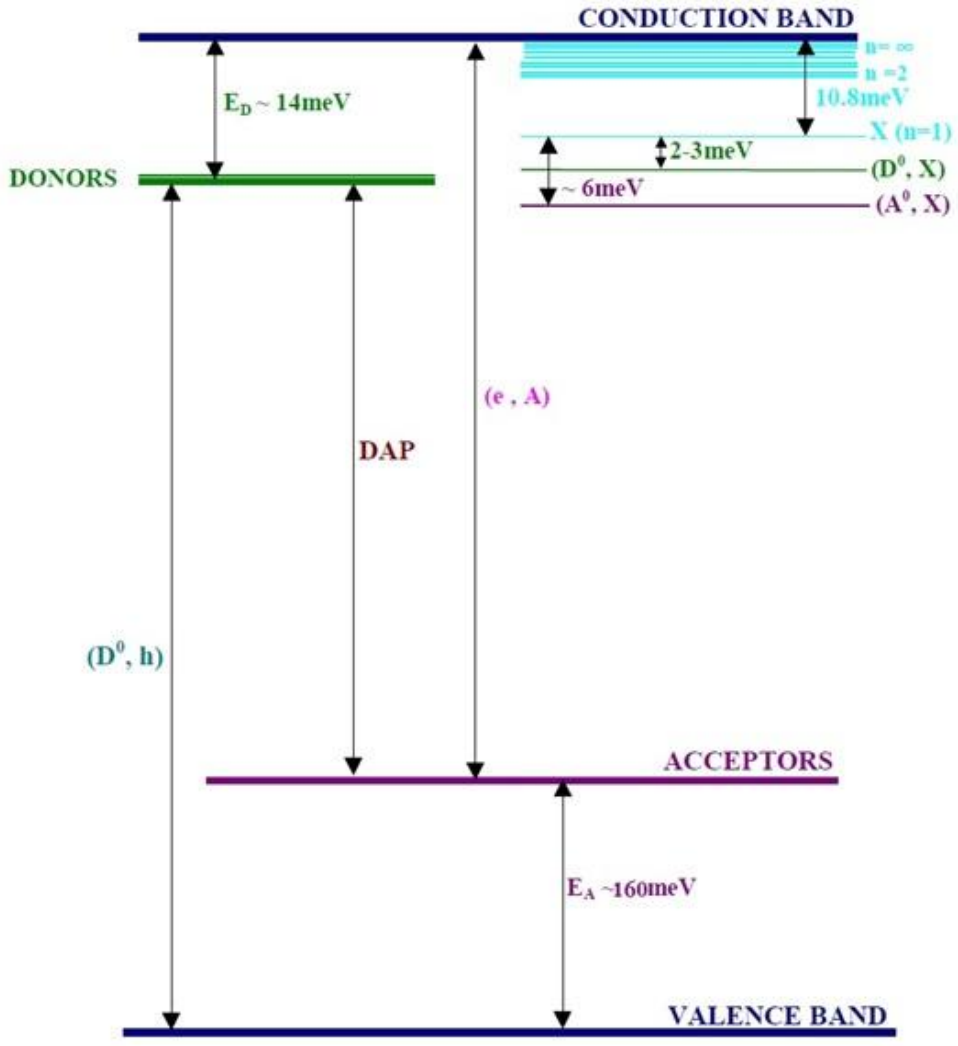

Figure 2.2 Several recombination processes in CZT

A common outcome of a non-radiative recombination is emission of phonons, the collective vibrational modes of the atoms in the crystal. These phonons can interact with electrons, holes or excitons and affect the photoluminescence spectra. Phonons can

appear in two modes acoustic or optical and for optical phonons we have longitudinal optical mode (LO) or transverse optical mode (TO). In CZT, it is reported that the direct electron phonon interaction is dominated by LO phonons and our calculation in chapter 4 restates these reports by measuring very low effective factors for other type of phonons. The LO phonon energy in CdTe is around 21 meV and for the purpose of our study, a value of 21.77 meV has been assumed for all samples from linear interpolation of CdTe LO phonon energy and ZnTe LO phonon energy.

X-Ray Diffraction

The best tool to detect ordered arrays of atoms separated by the distance of a covalent bond is X-ray diffraction. As the energy of electrons in the core orbitals of many types of atoms is approximately equal to the energy of a quantum of an X-ray radiation, these electrons will be the main source of scattering for this radiation. Atoms with a higher density of electrons in their orbitals scatter the radiation more strongly than atoms with less density of electrons. The interference of these scattered X-rays results in the phenomenon called diffraction.

Huygen’s principle is one of the main bases of diffraction theory. According to this principle, every point on a wavefront of a propagating wave, can be considered as a new origin of the wave, propagating with the same speed as the main wave. Figure 2.3 shows a point on a wavefront and the new wave origin that can be considered to be placed on that point[21].

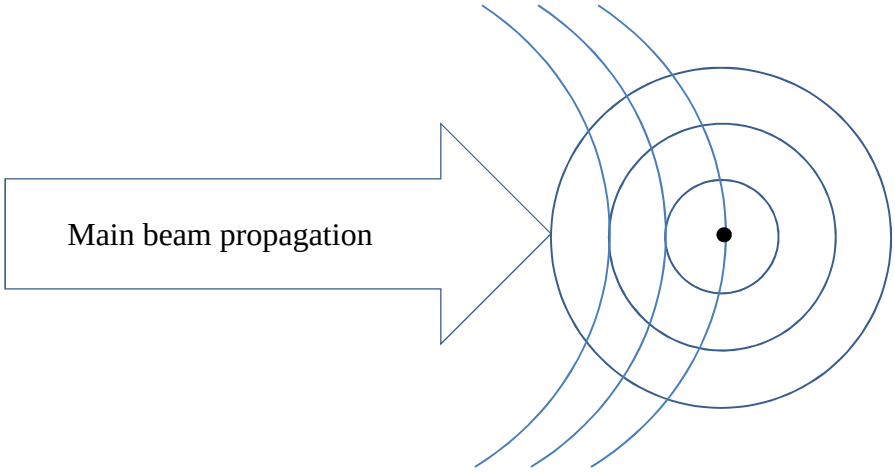

Figure 2.3 Huygen's principle. A new scattered wave origin is considered on the wavefront with the same wavelength and propagation speed as the main wave

Now if we consider two objects, called A and B, placed in front of a wavefront, each of these objects scatters the wave such that they act like new wave point sources for waves with the same speed and wavelength. The final observed waveform behind these objects depends on the spacing between these objects and the distance from A and B where we are observing the result. In some points the wave from object A and the one from object B interfere constructively, when they have same phase, and in some other points they interfere destructively, when they have opposite phase. This kind of interference is called diffraction. The resulting waveform carries information about the relative positions of A and B. This is how X-ray diffraction is used to determine structural features of crystals.

Bragg's law is the second basic principle of diffraction spectroscopy. It relates the diffraction to the relative distance between the scattering objects. For this purpose, consider a one dimensional crystal with reflection planes placed a distance d apart. An

incident X-ray beam hits these planes at an angle θ and is reflected with identical angle θ. The reflected beam from each plane has a different phase that is related to the extra path the beam traveled to reach that plane, in comparison to the beam reflected from higher or lower planes. Constructive interference of these beams observed in a distance much greater than d only happens whenever this extra path is equal to an integer number of wavelengths, so that the reflected beams have a similar phase. The extra path between a specific beam and the beam reflected from one plane higher is described as:

$$\frac{1}{2}\, P_{Extra} = d \sin\theta$$

Finally by assuming that the extra path is equal to an integer number of wavelengths:

$$2d \sin\theta = n\lambda$$

This equation relates the diffraction angle to the spacing between the objects and shows that there is a reciprocal relation between these two. In other word, larger spacing between the objects results in lower diffraction angles. In crystals, d can be interpreted as the lattice constant and the distance between the atoms in the lattice constant. Therefore changing θ will result in different peaks with different angles that characterize the features of the crystal structure.

3 Methods

In this chapter, a description of the equipment and systems that have been used in this work is presented.

Photoluminescence Setup

For performing photoluminescence tests at very low temperatures, an optical cryostat (CS202AI-DMX-1SS) from Advanced Research Systems Inc with optical windows was used. This system is connected to a helium gas compressor from the same company and a vacuum system consisting of a rough vacuum pump and a turbo pump provided a cold sample holder in vacuum with temperatures nominally as low as 4 K.

A laser setup consisting of a red pumping laser diode (Laser Diode Module 7200) from Spectra Physics connected to a radio frequency driver (Q-Switch Driver 7250) and a 532 nm green laser module (Model 7950-L104) was used as the excitation source for photoluminescence spectroscopy.

The laser beam was directed to the samples surface through the optical windows on the cryostat system by a prism. The radiated photoluminescence was collected through the same window by a custom optical setup made by optical lenses and filters from Thorlabs. The optical setup focused the excited point on the sample on a tip of a fiber optic cable and filtered light with wavelength below 600 nm, so that the excitation light from the laser does not affect the output signal. The fiber optic cable transferred the collected radiation to a spectrograph from Acton Research (SpectraPro 3000) where it was detected

with a liquid nitrogen cooled InGaAs array detector from Roper Scientific (Model 7410-0003).

Figure 3.1 shows a descriptive diagram of the setup for photoluminescence spectroscopy.

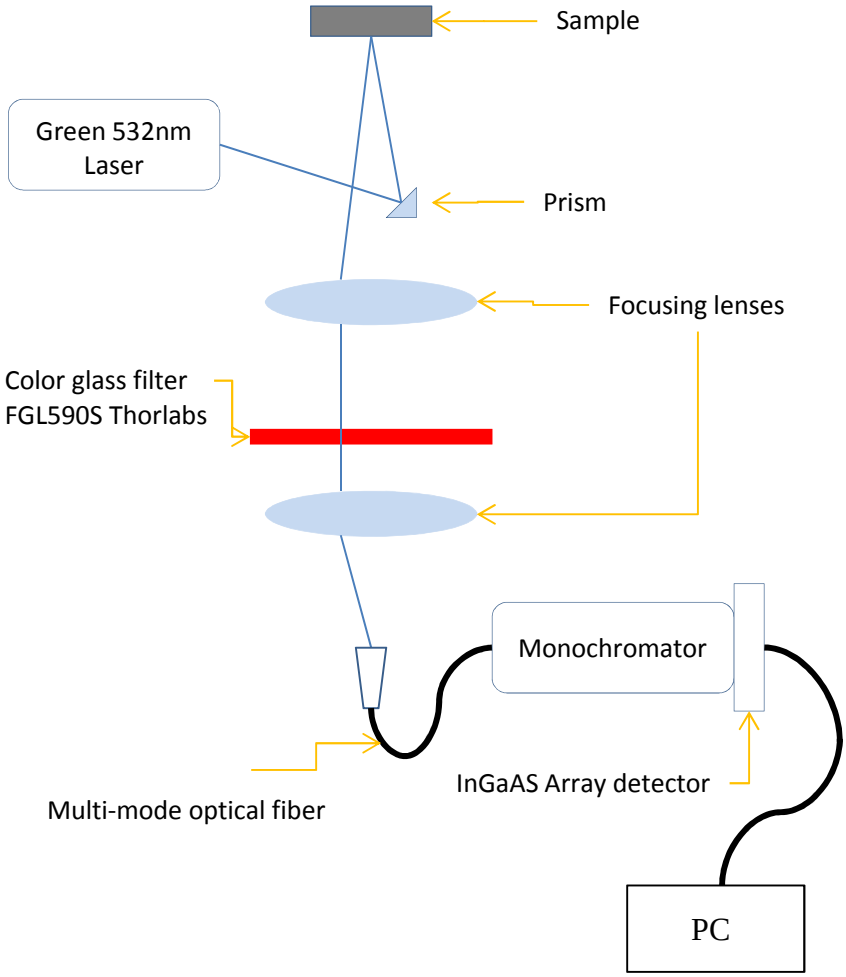

Figure 3.1 Photoluminescence setup diagram

X-ray Diffraction Setup

X-ray diffraction analyses in this work were carried out with a Bruker D8 Discover Diffactometer system, an advanced X-ray diffractometer for material science research applications. This system includes a Turbo X-ray source anode for maximum intensity. It is a copper X-ray source with X-ray wavelength of 1.54056 angstrom. The system also includes two different detector configurations, a crystal analyzer and a variable slit detector. The crystal analyzer gives a lower intensity with higher resolution of 15 arc seconds, while the variable slit provides a much stronger signal with lower resolution of 50 arc seconds. The sample holder stage allows movements with minimum step size of 0.01 mm in directions of x, y, z, and 0.001 degrees in phi – rotation of the sample holder around z axis – and chi – the rotation of the sample holder around x axis. The detector is also mounted on a precise mobile arm that allows angular changes as small as 0.0001 degree. Figure 3.2 shows D8 Discover.

Figure 3.2 Bruker D8 Discover X-ray diffractometer system

CdZnTe Samples

In this work, four different samples with nominal zinc molar concentration of 10%, which is the most common concentration used in detector grade CZT systems, have been provided by RedLen. There are a variety of qualities among these samples, so that defect and impurities features can be detected by comparison. The sample numbers are 2964, 3495, 1527, and 1218. Samples were prepared in cubic shapes of 1 cm × 1 cm × 0.5 cm and 1 cm × 1 cm × 0.3 cm. The surface was chemically and mechanically polished.

4 Results and Discussion

Photoluminescence studies

Low temperature photoluminescence spectroscopy has been done on four different samples of $Cd_{1-x}Zn_xTe$ (x=0.1) and the resulting spectra have been analysed in order to characterize several features of the crystal including its impurities, dislocations, defects density, and composition. A typical photoluminescence spectrum of a CdZnTe crystal at low temperature is shown in figure 4.1.

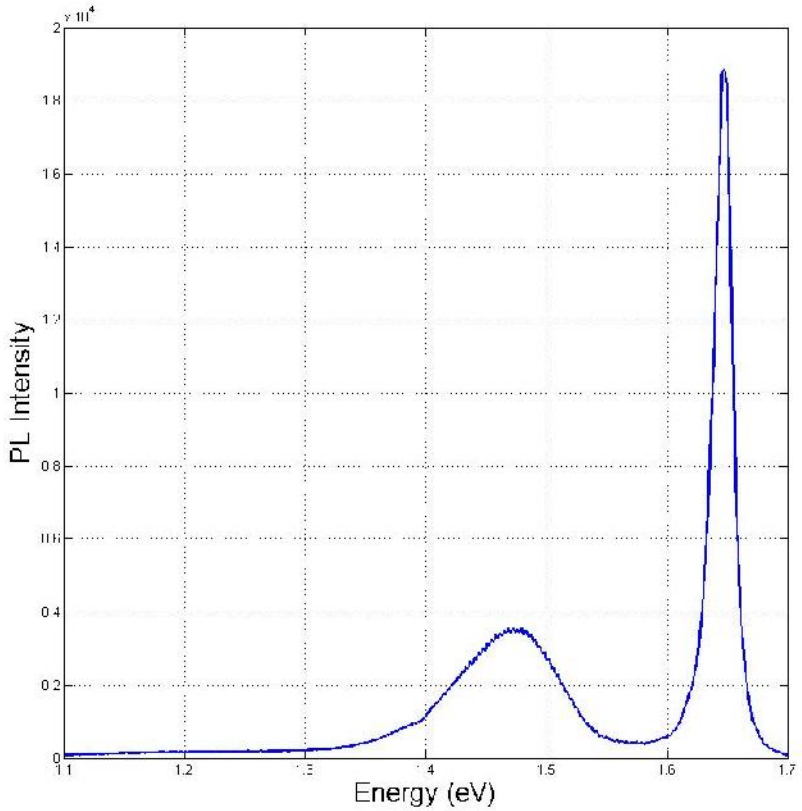

Figure 4.1 Photoluminescence spectrum of CZT at 10K temperature. The kink at 1.4 eV is caused by inaccuracy in the spectral calibration of the spectrometer

The sharp peak in the spectrum is the donor-bound exciton (D^0,X) emission at 10K. The broader peak for the deep-level band at around 1.47 eV is attributed to donor-acceptor-pair recombination which is related to a level in which both donor and acceptor units are available in close vicinity of each other. Indium A-center acceptor levels can contribute to this peak as well. It has been reported that in CZT, a cadmium vacancy, the most typical structural defect in CZT, can be occupied by an indium atom and forms an In_{Cd} that behaves as a shallow donor state. Furthermore, various complexes such as a positively ionized indium placed at a cadmium vacancy surrounded by a double negatively ionized cadmium vacancy [In_{Cd}^{+} V_{Cd}^{2-}] that behaves as an ionized acceptor, and two positively ionized indiums placed at two cadmium vacancies surrounding a double negatively ionized cadmium vacancy [$2In_{Cd}^{+}V_{Cd}^{2-}$] as a neutral entity can be formed in presence of indium[22]. These complexes are created due to the self-compensation process that occurs when high concentration of indium is present and decreases the doping efficiency of the crystal[22]. Some of the samples' show a weak peak at around 1.61 eV at low temperature that can be attributed to acceptor-bound exciton emission. The presence of this peak shows that the concentration of acceptor units is relatively higher in these samples compared to the ones that did not show the aforementioned peak. Different structures can be considered as an acceptor in CZT other than typical acceptor atoms. Several defects and complexes involving cadmium vacancies in the crystal structure show behaviour similar to acceptor atoms. Another type of cadmium vacancy based complex that has been reported by Worschech et al.[23] is the reason for the appearance of another photoluminescence peak at around 1.58 eV and it is

called a C-line. This peak is attributed to an exciton bound to an isoelectronic defect complex consisting of two indium atoms on cadmium vacancies and a cadmium vacancy shown in figure 4.2[23].

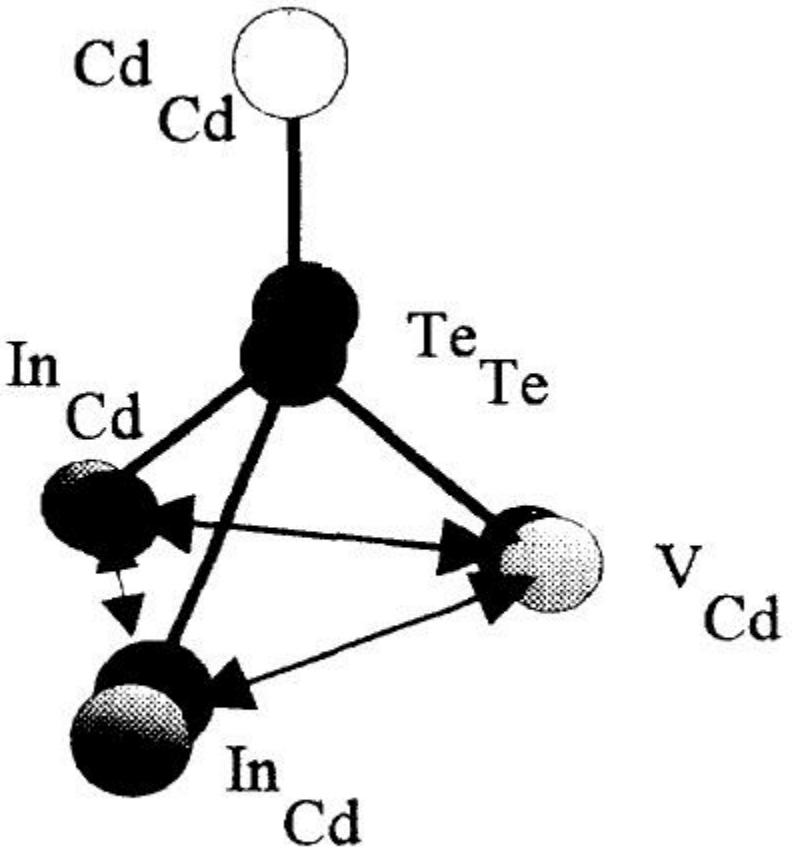

Figure 4.2 An In_{Cd}-V_{Cd}-In_{Cd} defect complex created by self-compensation of indium in CdZnTe and acts as a shallow acceptor

We used the least squares method to fit for our experimental data to equations in the literature. In this method, we minimize the squares of the deviations between the fitted value and our experimental data. Furthermore, we reduce the degrees of freedom in our fits by fixing the value of some of the parameters, whenever the physical explanation of that parameter predicts a negligible change for it among our samples. For example, in the fit of the full-width-at-half-maximum of the photoluminescence peak we expect negligible changes in the exciton-LO phonon coupling constant due to the small composition variations in our samples, the value for this parameter has been fixed.

As typical of other semiconductor alloys, the band gap and free-exciton energies in a ternary compound such as CZT depend on the zinc molar concentration. This dependence can be explained by the change in the lattice constant due to incorporation of zinc in the CdTe crystal. The more zinc in the crystal, the smaller the lattice constant. The repulsive interaction of core electrons will increase when the inter-atomic spacing decreases and this increase in repulsive interaction increases the band gap. Several expressions in the literature tried to estimate the relation between the band gap E_g and zinc molar concentration x. A list of these expressions is presented below and their estimation for each sample has been listed in table 4.1. The resulting zinc molar concentrations from X-ray analysis that are presented in the next section is also listed in this table for comparison purposes. In these measurements the band gap energy has been determined from the photoluminescence spectrum of the samples at lowest temperature.

1. Eg (12 K) = 1.598 + 0.614x + 0.166x2 (eV) [Olego 1985][8] (0<x<1)
2. Eg (9 K) = 1.604 + 0.42x + 0.33x2 (eV) [Chen 1991][24] (0<x<0.1)
3. Eg (4.2 K) = 1.606 + 0.322x + 0.463x2 (eV) [Reno 1992][25] (0<x<1)
4. Eg (4.2 K) = 1.6058 + 0.546x (eV) [Tobin 1995][26] (0.03<x<0.06)
5. Eg (2 K) = 1.606 + 0.522x + 0.26x2 (eV) [Magnea 1994][27] (0<x<1)
6. Eg (x) = 1.606 + 0.520x + 0.254x2 (eV) [Franc, 2000][14] (0<x<0.06)

Table 4.1 Zinc molar concentraition estiamtion

Sample	E_g	Olego	Chen	Reno	Tobin	Magnea	Franc	X-ray
1218	1.651	0.08439	0.10348	0.11929	0.08278	0.08279	0.08316	0.0883
1527	1.650	0.08283	0.10143	0.11697	0.08095	0.08102	0.08138	0.0843
2964	1.657	0.09371	0.11567	0.13296	0.09377	0.09335	0.09378	0.0939
3495	1.656	0.09216	0.11365	0.13071	0.09194	0.09160	0.09201	0.0891

A detailed photoluminescence study of four different CZT samples has been done for samples for different temperatures varying from 8K to 300K. Figures 4.3 through 4.6 show the temperature dependence of the photoluminescence of these samples.

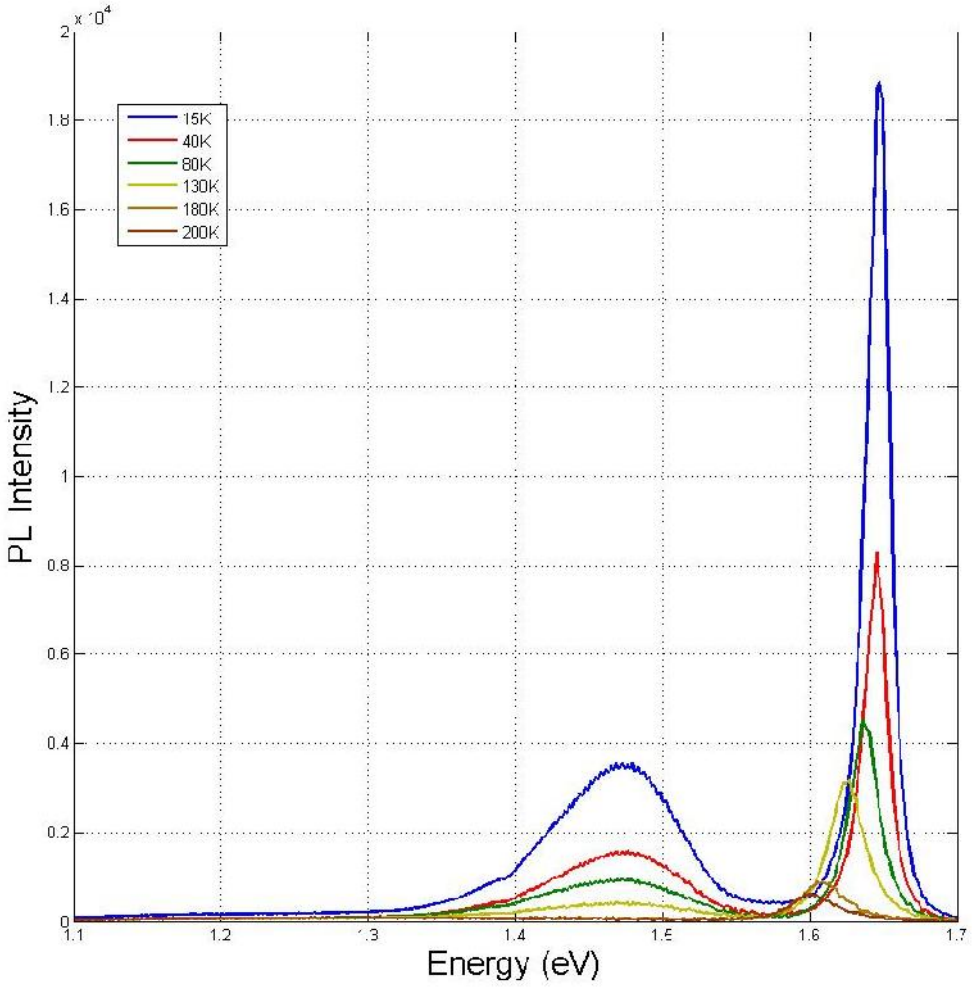

Figure 4.3 Temperature dependence of photoluminescence spectrum for sample 1218

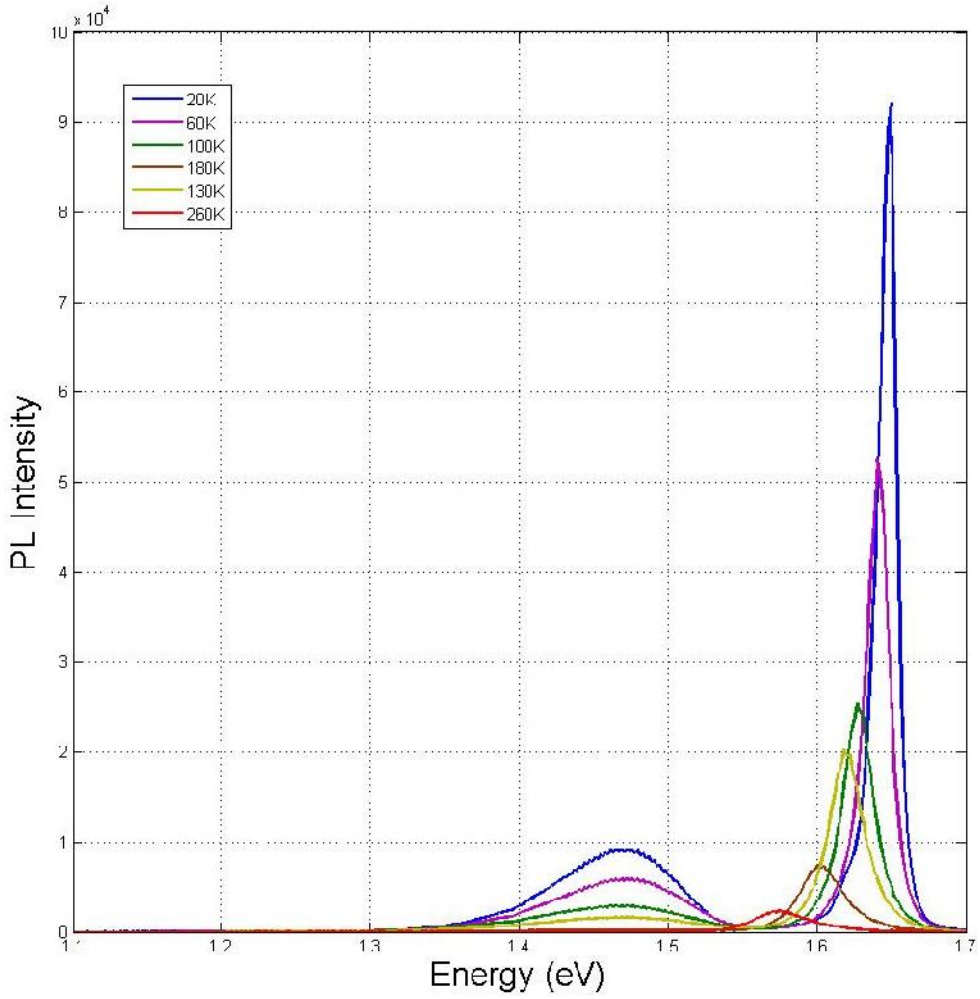

Figure 4.4 Temperature dependence of photoluminescence spectrum for sample 1527

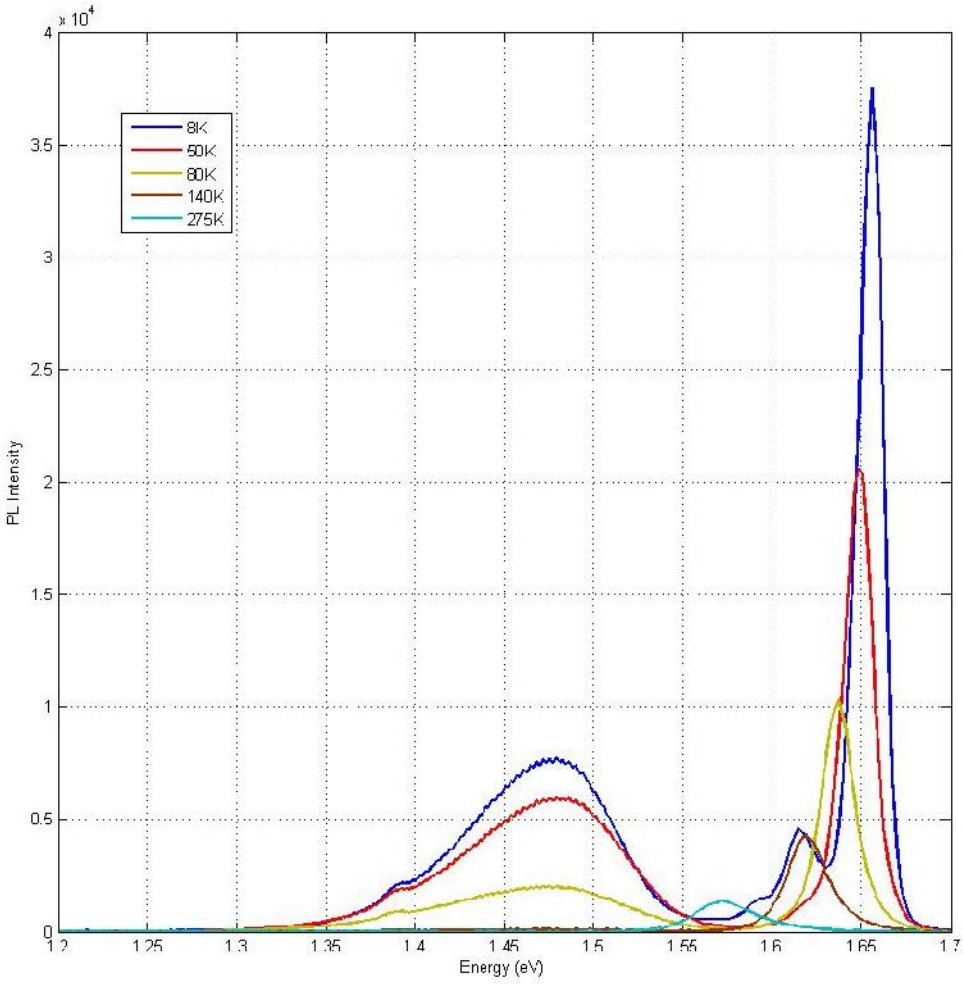

Figure 4.5 Temperature dependence of photoluminescence spectrum for sample 2964

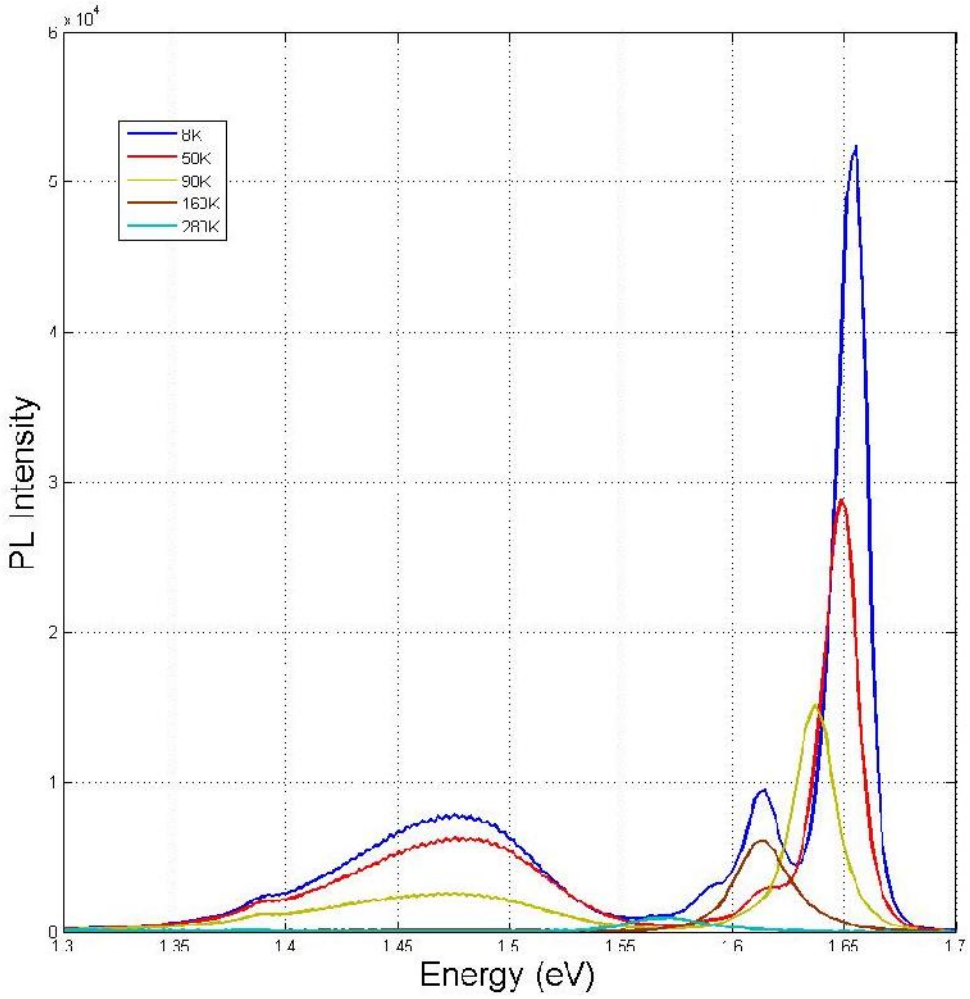

Figure 4.6 Temperature dependence of photoluminescence spectrum for sample 3495

There are several features that are distinguishable in the temperature dependence of the samples' photoluminescence. The acceptor-bound exciton emission peak which is present in only two of the samples is thermally quenched quickly when the temperature raised. All of the peaks show a thermal quenching effect that will be studied in detail further in this study. Furthermore, red-shift or shift of the peak energy to lower energies is visible

in the spectrum of all samples. This effect can be translated to a band gap shift with temperature that will be studied in detail. The donor-bound exciton peak probably evolves to a donor-to-valence band transition at higher temperatures. The full width at half maximum (FWHM) of the donor-bound exciton peak is also important as it gets broader at higher temperatures. This effect and its origin, which is mainly from defect and structural inhomogeneity, will be studied in detail further in this study.

Three different expressions have been reported for the variation of the band gap energy with temperature in semiconductors.

$$E_g = E_0 - \alpha \frac{T^2}{(T+\beta)}$$

where α and β are constants[28].

$$E_g = E_0 - \frac{\alpha T^2 + \vartheta}{T+\beta}$$

where α, β and ν are constants. This equation is called modified Varshni's equation[28].

$$E_g = E_0 - \frac{\alpha}{e^{\frac{\theta_E}{T}} - 1}$$

where α is a constant related to exciton-LO phonon coupling and θ_E is called Cody temperature[29].

Fitting the data acquired by photoluminescence spectroscopy of the samples with these equations gives the constants related to each sample. As it has been shown by Chichibu et al, 1997 that if optical phonon branches of a polar semiconductor is next to the acoustic ones in energy, then fitting the temperature dependence of the band gap energy using the Cody equation that assume Einstein phonons is better than using the Varshni fitting that

assumes Debye phonons. Therefore, the fitting for all three equations is shown in figure 4.6 only for one sample for the sake of comparison and for the other samples only the Cody fitting has been shown in figure 4.8 through 4.10.

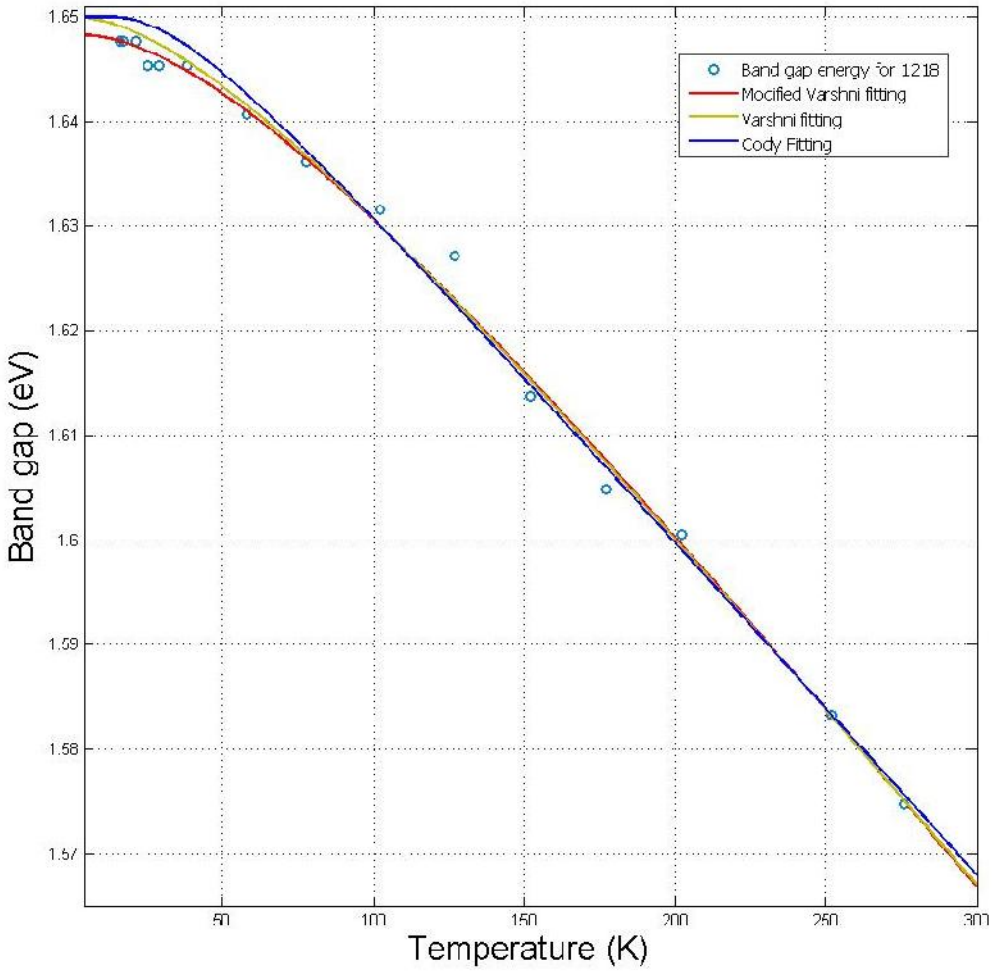

Figure 4.7 Temperature dependence of band gap energy for sample 1218 fitted with all three equations

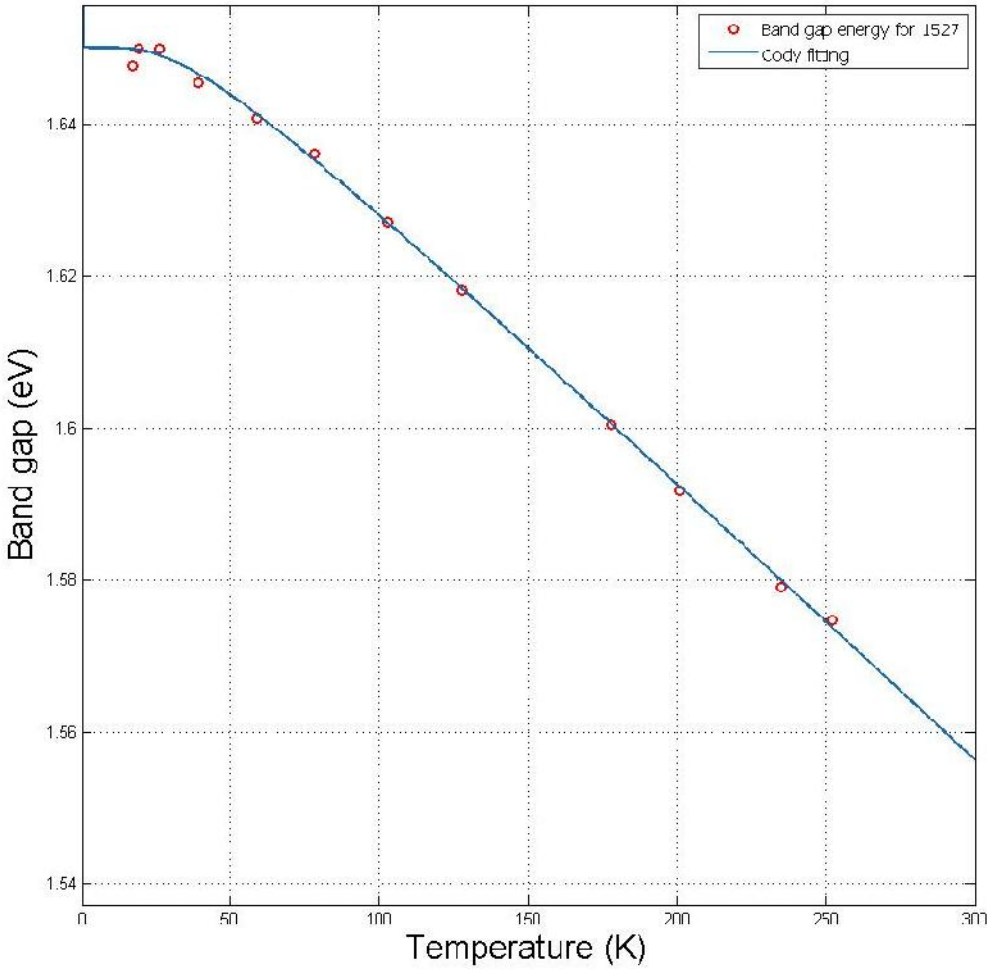

Figure 4.8 Temperature dependence of band gap energy for sample 1527 fitted with the Cody equation

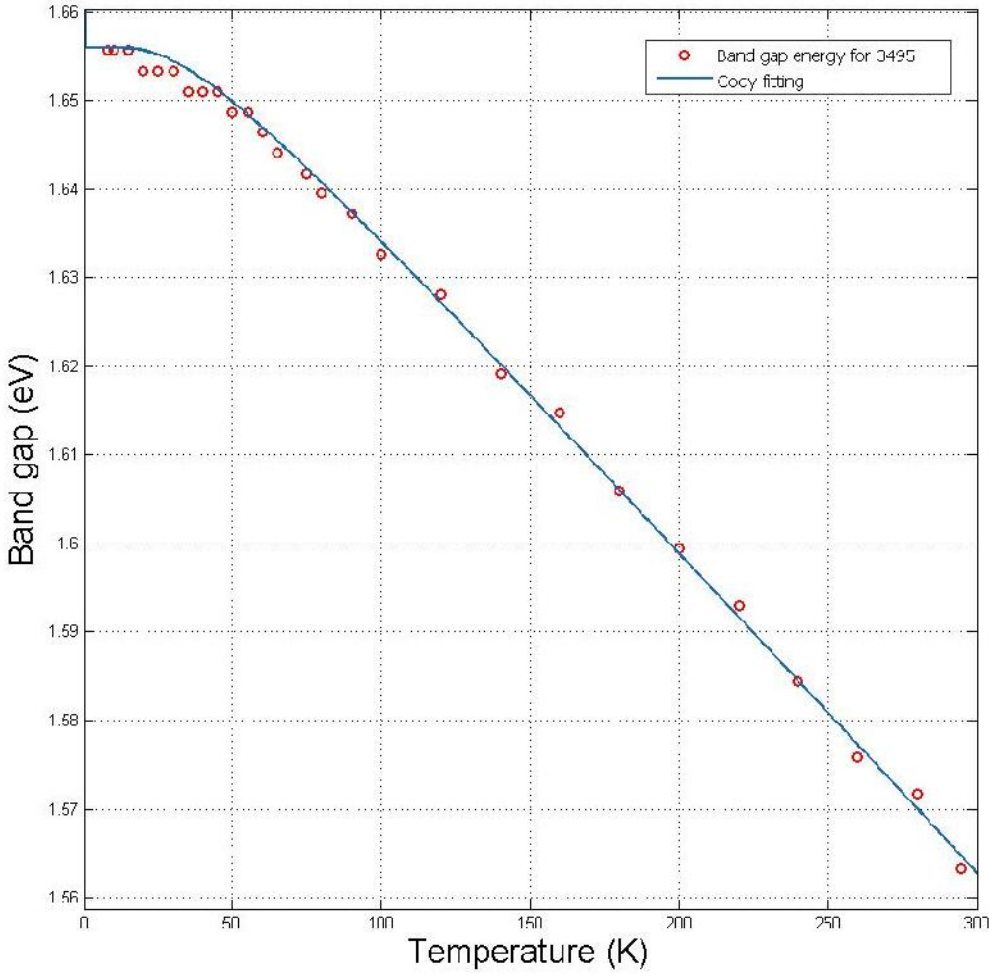

Figure 4.9 Temperature dependence of band gap energy for sample 3495 fitted with the Cody equation

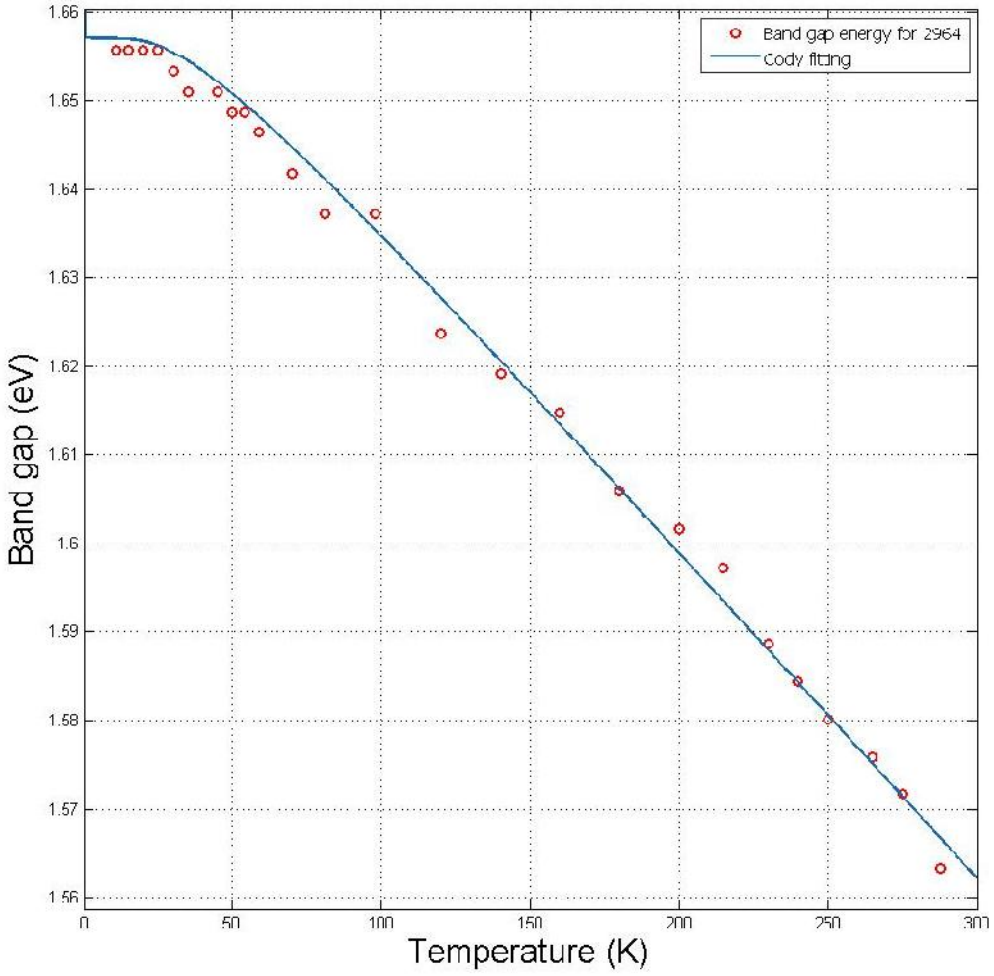

Figure 4.10 Temperature dependence of band gap energy for sample 2964 fitted with the Cody equation

Measured parameters for all of the fittings have been shown in table 4.2. The same Cody temperature has been implemented for all of the samples as the fitting results were very close to each other. Also, the band gap energy at T = 0K has been estimated from the photoluminescence spectrum at low temperatures.

Table 4.2 Fitting parameters for temperature dependence of band gap energy

	Varshni	Varshni's modification	Cody
Sample 1218			
E_0	1.650 (eV)	1.650 (eV)	1.650 (eV)
α	0.0003518 (eV/K^2)	0.000364 (eV/K^2)	0.03019 (eV)
β	81.6 (K)	95.9 (K)	-
ν	-	0.168 (eV)	-
θ_E	-	-	94 (K)
Sample 1527			
E_0	-	-	1.650 (eV)
α	-	-	0.03448 (eV)
β	-	-	-
ν	-	-	-
θ_E	-	-	94 (K)
Sample 2964			
E_0	-	-	1.657 (eV)
α	-	-	0.03488 (eV)
β	-	-	-
ν	-	-	-
θ_E	-	-	94 (K)
Sample 3495			
E_0	-	-	1.656 (eV)
α	-	-	0.03430 (eV)
β	-	-	-
ν	-	-	-
θ_E	-	-	94 (K)

The exciton-LO phonon coupling constant that has been measured here using the Cody equation is used in fitting the temperature dependence of the FWHM of the photoluminescence peak, as the broadening factor of exciton-LO phonon interactions uses the same form.

There are several factors that account for broadening of the photoluminescence peak at higher temperatures. In general, this broadening has two parts that separate the temperature dependent and temperature independent terms. The temperature independent

term is mainly due to the inhomogeneity of the crystal. It is a constant and it only depends on the structure of the crystal. However, the temperature dependent term consists of three terms: one for the broadening effect of acoustic phonon-exciton interactions at higher temperatures, one for the broadening effect of optical phonon-exciton interactions at higher temperatures, and one for the broadening effect of defect and impurity centers thermally activated at higher temperatures. Therefore, this expression has been reported to predict the FWHM of a photoluminescence peak at different temperatures[30]:

$$\Gamma(T) = \Gamma_{\text{inh}} + \gamma_{\text{LA}} T + \frac{\Gamma_{\text{LO}}}{\exp(\hbar\omega_{\text{LO}}/k_{\text{B}}T) - 1} + \Gamma_{\text{i}} \exp(E_{\text{i}}/k_{\text{B}}T)$$

where Γ_{inh} is the inhomogeneous broadening term, γ_{LA} is a coefficient of exciton-acoustic phonon interaction, Γ_{LO} is the exciton-LO phonon coupling constant, $\hbar\omega_{LO}$ is the LO phonon energy, Γ_i is a proportionality factor which accounts for the concentration of impurity centers, and E_i is the binding energy of impurity-bound excitons averaged over all possible locations of the impurities. Using this equation to fit the experimental data we gathered results in a set of fittings and parameters that are shown in figure 4.11 to 4.14 and table 4.3. Γ_{LO} is supposed to be constant in all samples, as the composition variation of the samples is small and exciton-LO phonon interactions changes among the samples is expected to be small. The coupling constant measured from the Cody equation has been used for Γ_{LO}. Furthermore, E_i is also considered to be constant for all samples and its value has been estimated from the average of the fitted data. $\hbar\omega_{LO}$ variation among all four samples considered to be negligible and a linear interpolation of LO phonon energies of CdTe and ZnTe has been used to estimate its value.

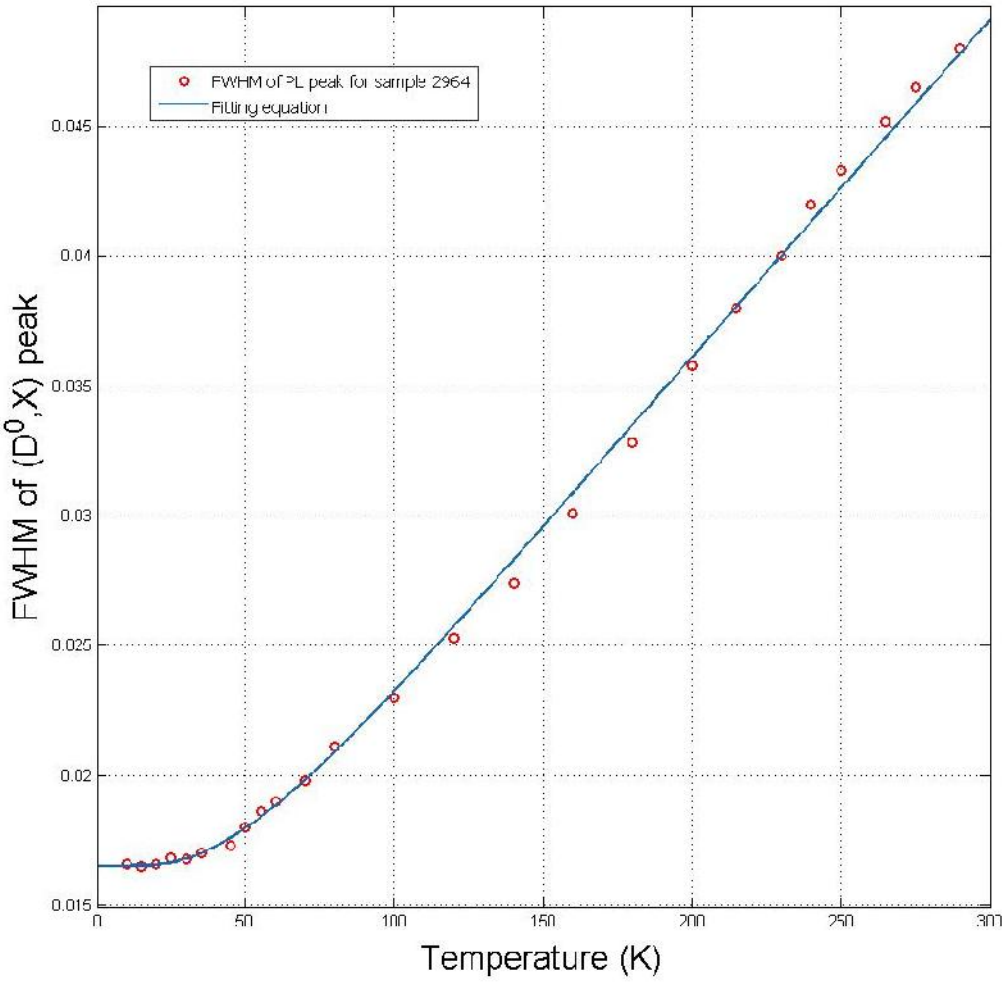

Figure 4.11 Temperature dependence of photoluminescence (D^0,X) peak full width at half maximum for sample 2964

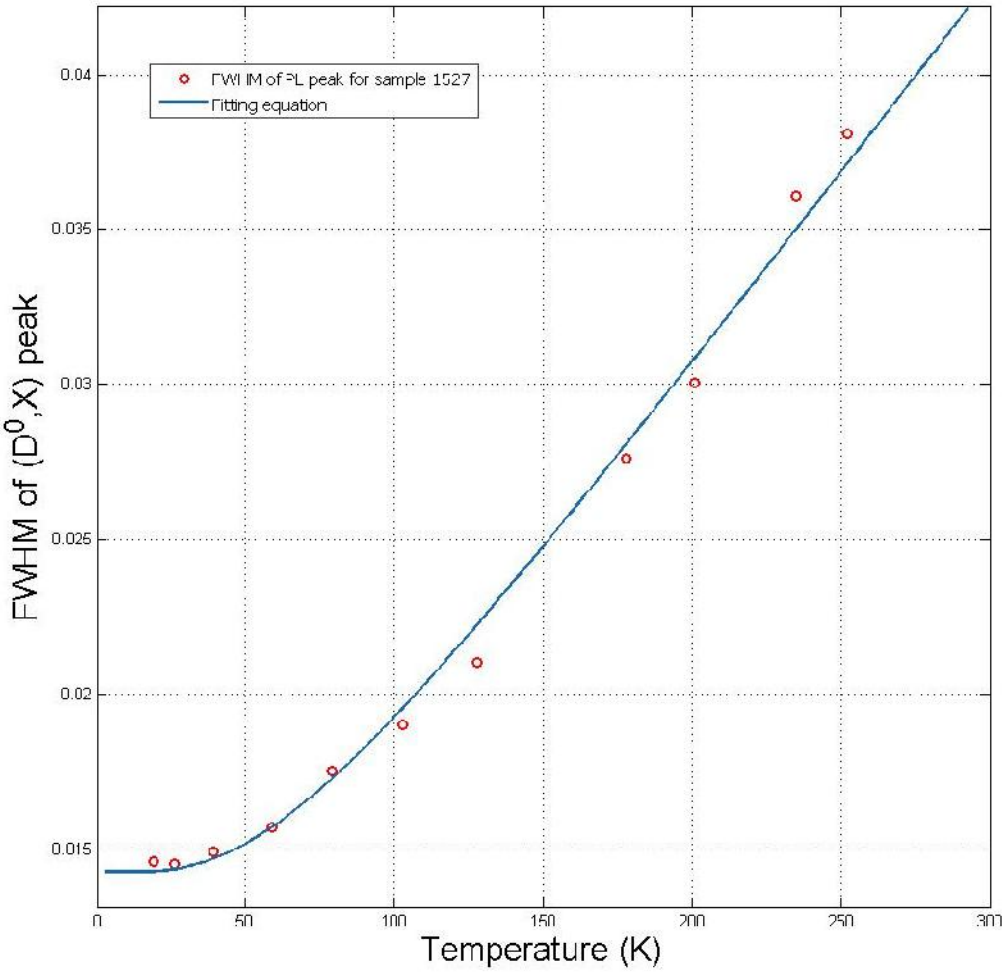

Figure 4.12 Temperature dependence of photoluminescence (D^0,X) peak full width at half maximum for sample 1527

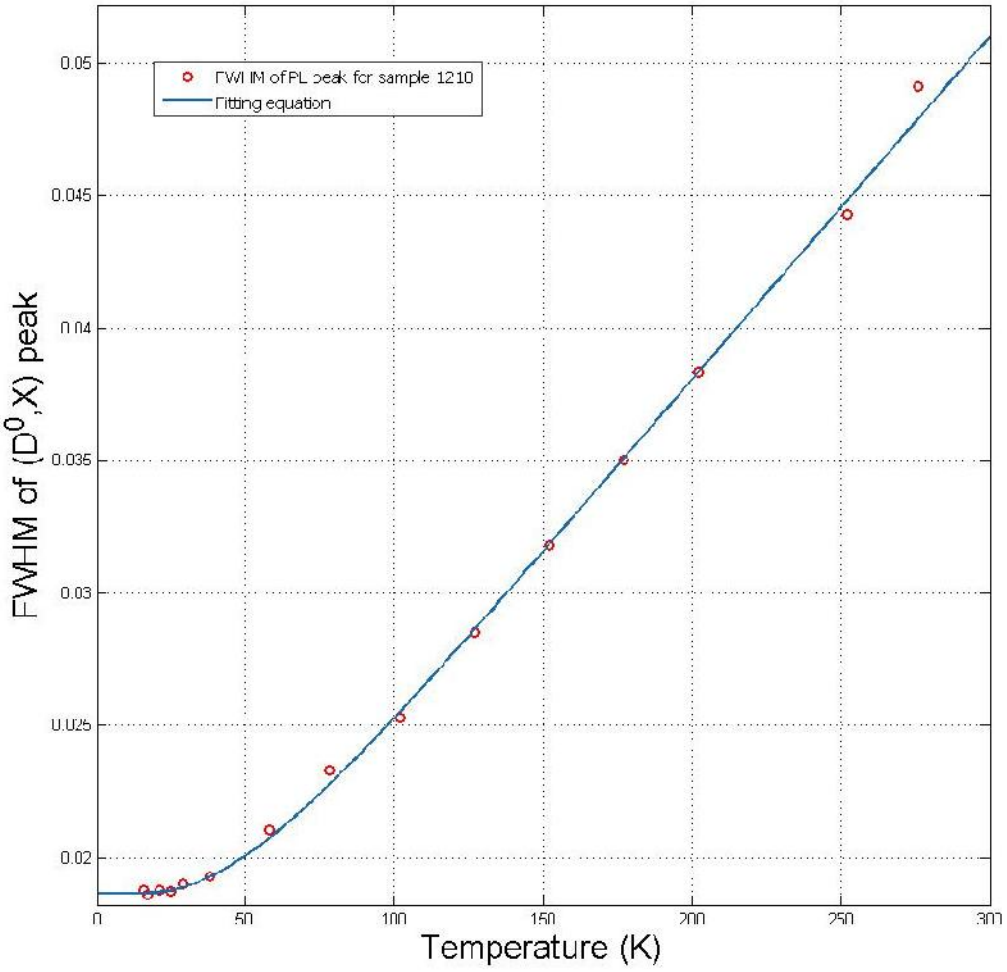

Figure 4.13 Temperature dependence of photoluminescence (D^0,X) peak full width at half maximum for sample 1218

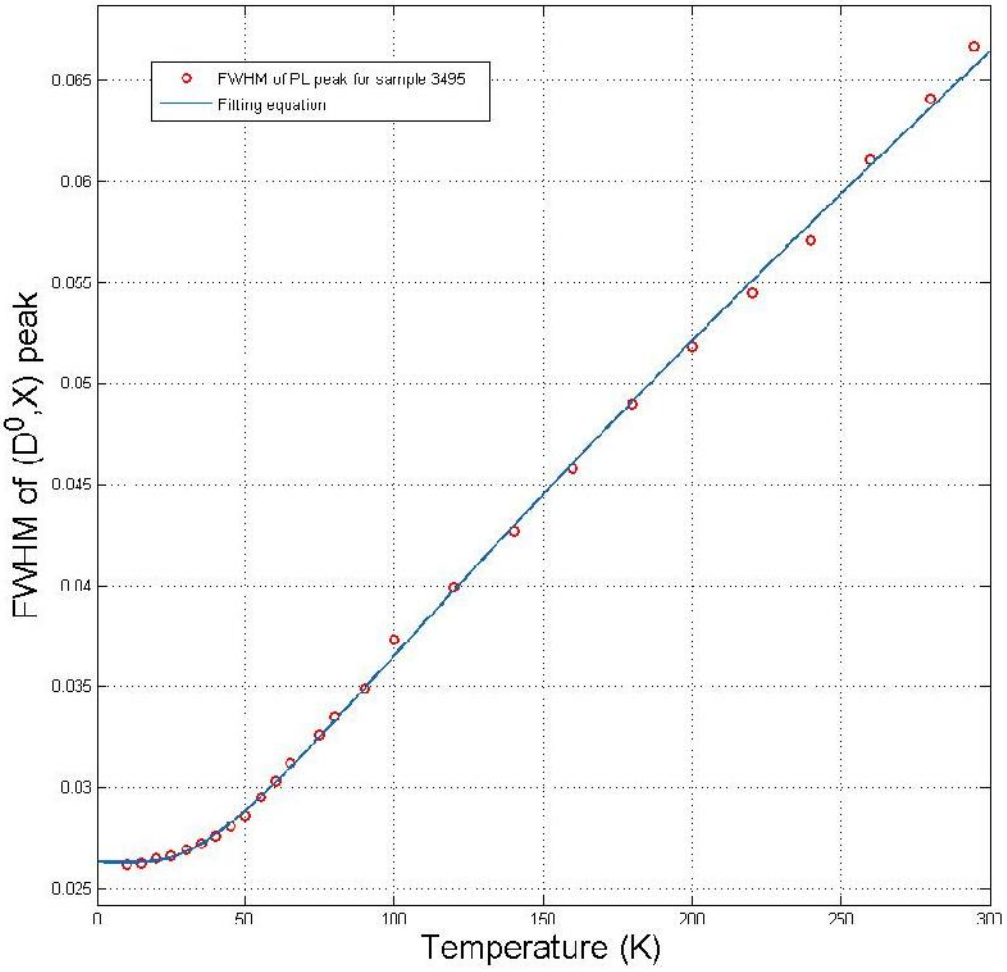

Figure 4.14 Temperature dependence of photoluminescence (D^0,X) peak full width at half maximum for sample 3495

Table 4.3 Temperature dependence of photoluminescence (D^0,X) peak FWHM fitting parameters

Sample	1218	1527	2964	3495
E_i	8.1 meV	8.1 meV	8.1 meV	8.1 meV
Γ_i	12.4 meV	7.2 meV	12.7 meV	23.8 meV
$\hbar\omega_{LO}$	21.77 meV	21.77 meV	21.77 meV	21.77 meV
Γ_{LO}	31.6 meV	31.6 meV	31.6 meV	31.6 meV
Γ_{inh}	18.7 meV	14.3 meV	16.5 meV	26.3 meV

As the fitting parameters show, sample 1527 has the lowest values for the broadening factors due to impurity centers concentration and crystal inhomogeneity. Samples 1218 and 2964 show similar values for the factor of impurity centers concentration, but the inhomogeneity broadening of sample 1218 is higher than sample 2964. Sample 3495 has the highest values of these factors, therefore it is assumed that it has the highest impurity concentration and inhomogeneity in its structure. This is in agreement with the fact that sample 3495 shows the strongest photoluminescence peak for (A^0,X) at low temperature, while other samples show no peak at all or a smaller peak.

Thermal quenching of photoluminescence peak intensity has been studied extensively in the literature. The temperature dependence of the peak intensity is usually depicted in a plot that shows intensity versus inverse of temperature 1/T. The data for temperatures lower than 60K-70K is usually fitted with this expression: [E. Cohen et al, 1983]

$$I(T) = \frac{I_0}{1 + C_1 e^{-\frac{E_1}{kT}} + C_2 e^{-\frac{E_2}{kT}}}$$

where E_1 and E_2 are the higher- and the lower-temperature activation energies, respectively. As our data is in the temperature range 8K-300K, we added another term for a new term to this equation and used it for fitting our data. The resulting equation that has been used for fitting is shown below:

$$I(T) = \frac{I_0}{1 + C_1 e^{-\frac{E_1}{kT}} + C_2 e^{-\frac{E_2}{kT}} + C_3 e^{-\frac{E_3}{kT}}}$$

The fits and data plots are shown in figure 4.15 to 4.18. The fitting parameters that have been used for these fitting are shown in table 4.4.

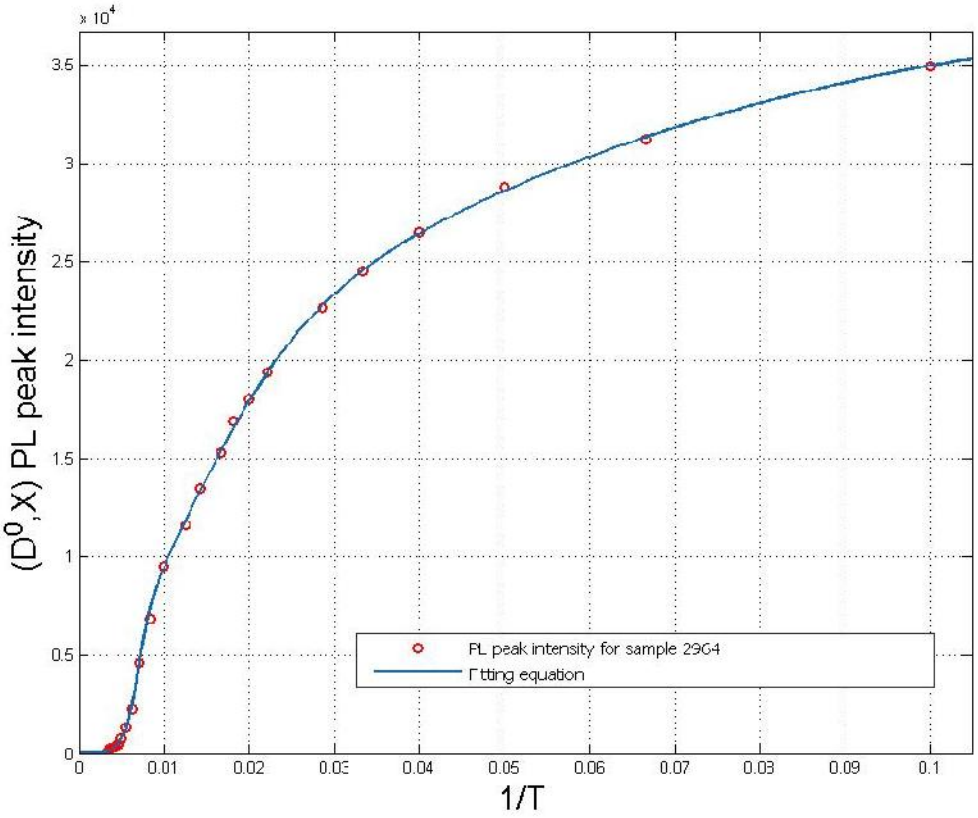

Figure 4.15 The temperature dependence of the photoluminescence (D^0,X) peak intensity for sample 2964

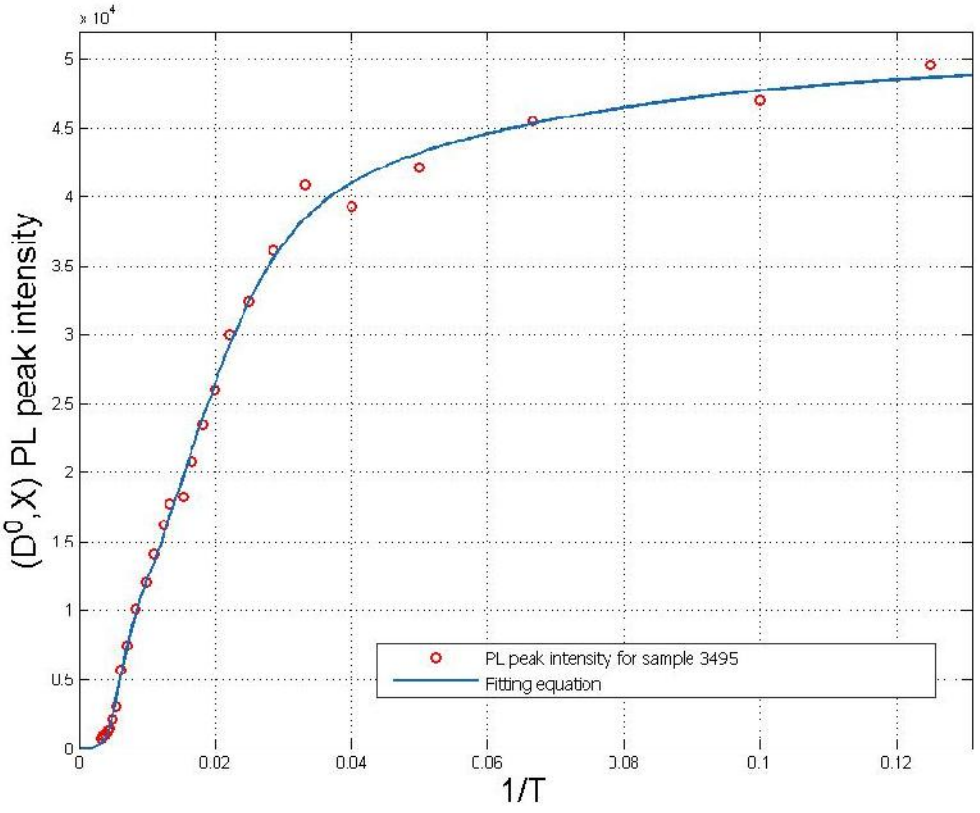

Figure 4.16 The temperature dependence of the photoluminescence (D^0,X) peak intensity for sample 3495

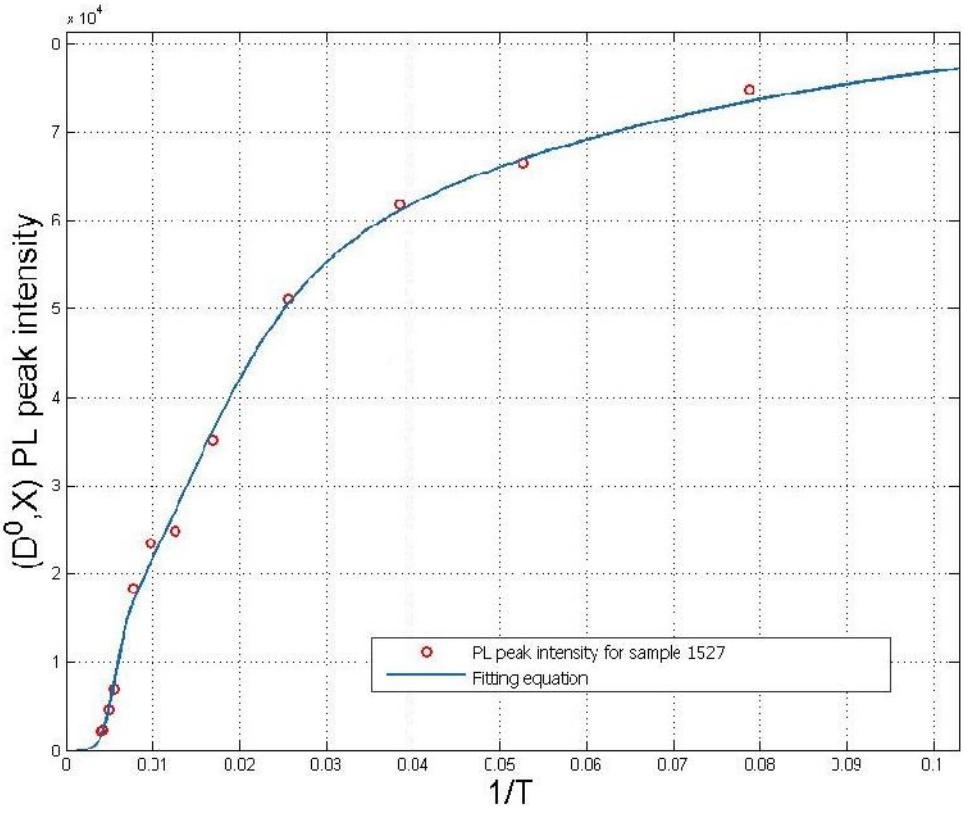

Figure 4.17 The temperature dependence of the photoluminescence (D^0,X) peak intensity for sample 1527

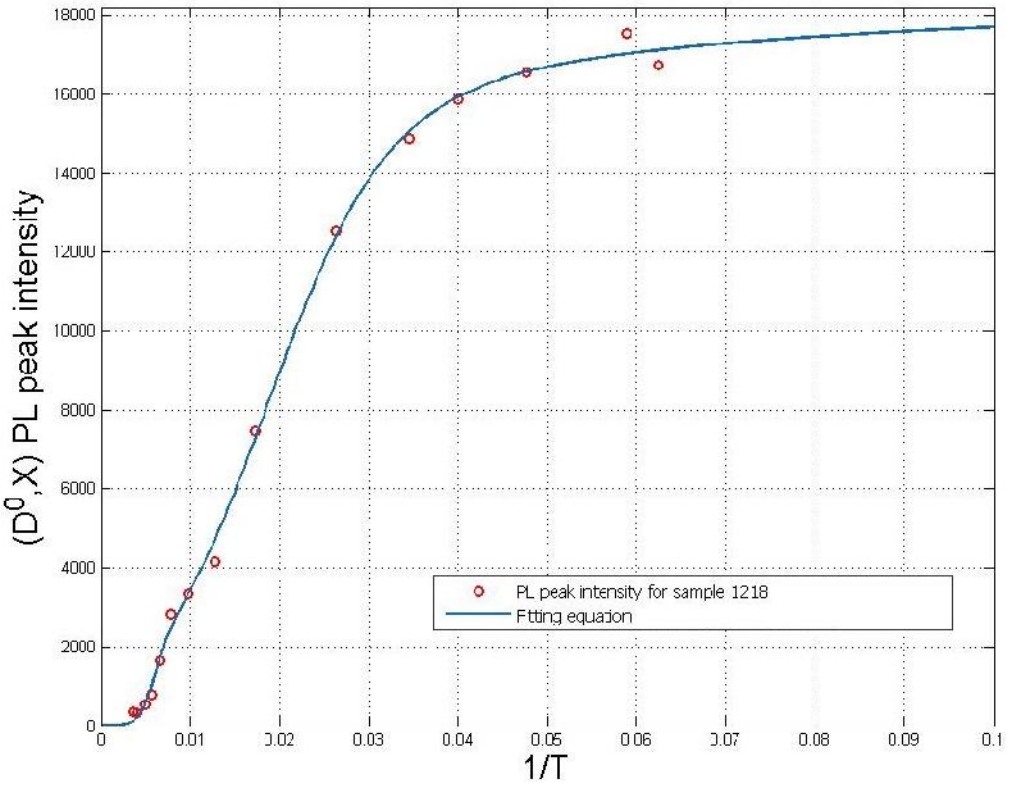

Figure 4.18 The temperature dependence of the photoluminescence (D^0,X) peak intensity for sample 1218

Table 4.4 Fitting parameters for the temperature dependence of the (D^0,X) peak intensity

Sample	1218	1527	2964	3495
E_1 (meV)	2.08	2.08	2.08	2.08
E_2 (meV)	13.29	13.29	13.29	13.29
E_3 (meV)	113.5	126.7	106.5	104.7
C_1	0.25	0.81	1.15	0.5
C_2	18.93	10.02	9.68	12.56
C_3	15850	17910	21670	6068

Values for E_1 and E_2 have been selected to be constant and the same for all samples, as their fitted values were close to each other and in the error range of the value. Also as it is considered that the processes associated with these energies are the same in all samples, it is a reasonable assumption. The quality of fitted data shows that forcing these parameters to be constant did not hinder the fitting process.

There are several dissociation processes that results in thermal quenching of the photoluminescence peak. Considering these processes, we concluded that the activation energy of 2.08 meV is due to the binding energy of exciton to donors. It is reported that the binding energy of exciton and donors is in range of 2-3 meV and this result is in agreement with the reported values. The free exciton energy in CdTe is reported to be 10.8 meV and activation energy of 13.29 meV is interpreted to be associated to a process in which a donor-bound exciton is freed and then the free exciton dissociates. This conclusion results to a free exciton energy of 13.29 - 2.08 = 11.21 meV that is acceptable for free exciton energy in CdZnTe crystal. The third activation energy in the range of 104.5-126.7 meV is in the range of reported activation energies for A-centers in CdZnTe and suggests that at higher temperatures, these impurity centers get thermally activated and provide a non-radiative recombination center for excitons and reduce the radiation intensity. At higher temperatures several kinds of recombination centers get thermally active and the third activation energy is attributed to average of all of these recombination centers and the variation of this energy among four samples can be explained by the fact that this energy is probably including other activation energies for other recombination centers that can be different for each sample.

X-Ray diffraction studies

X-Ray diffraction studies have been done on all samples on different spots of the samples. The samples show varying mis-cut among them as it seems that the crystal orientation does not affect the detector performance significantly. A wide ω/2θ scan, a wide 2θ/ω scan and a focused 2θ/ω scan on the (111) peak of all of the samples are shown in figure 4.19 and 4.24. The parameter ω is the angle between the crystal surface normal and the incident beam, while 2θ is the angle between the incident beam and the reflected beam. The parameter ω can be equal to θ if there is no mis-cut present for the sample and the crystal surface normal is parallel to the (111) vector. However, in presence of any mis-cut, ω will be equal to θ subtracted by the mis-cut value. The reciprocal mappings of samples 1527 and 3964 over the (111) peak are shown in figures 4.25 and 4.26.

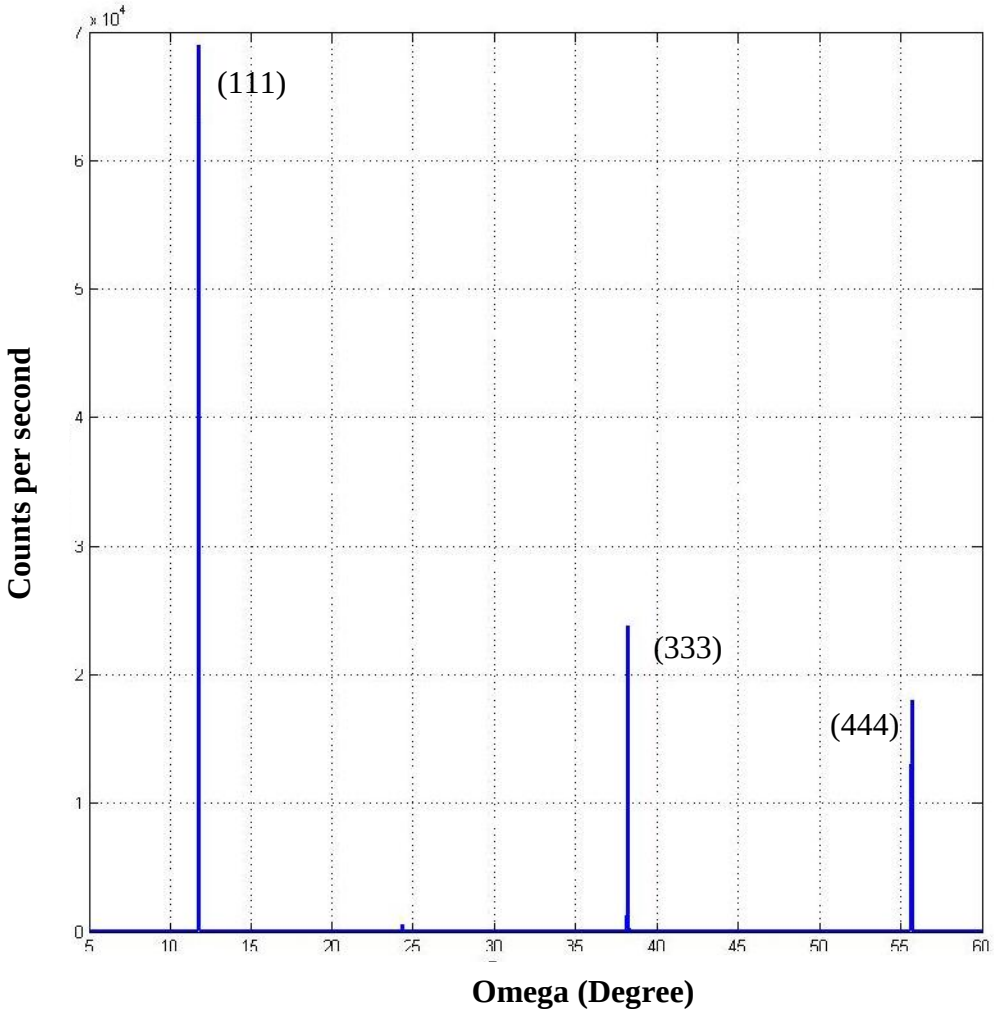

Figure 4.19 A wide ω/2θ XRD scan on sample 1218

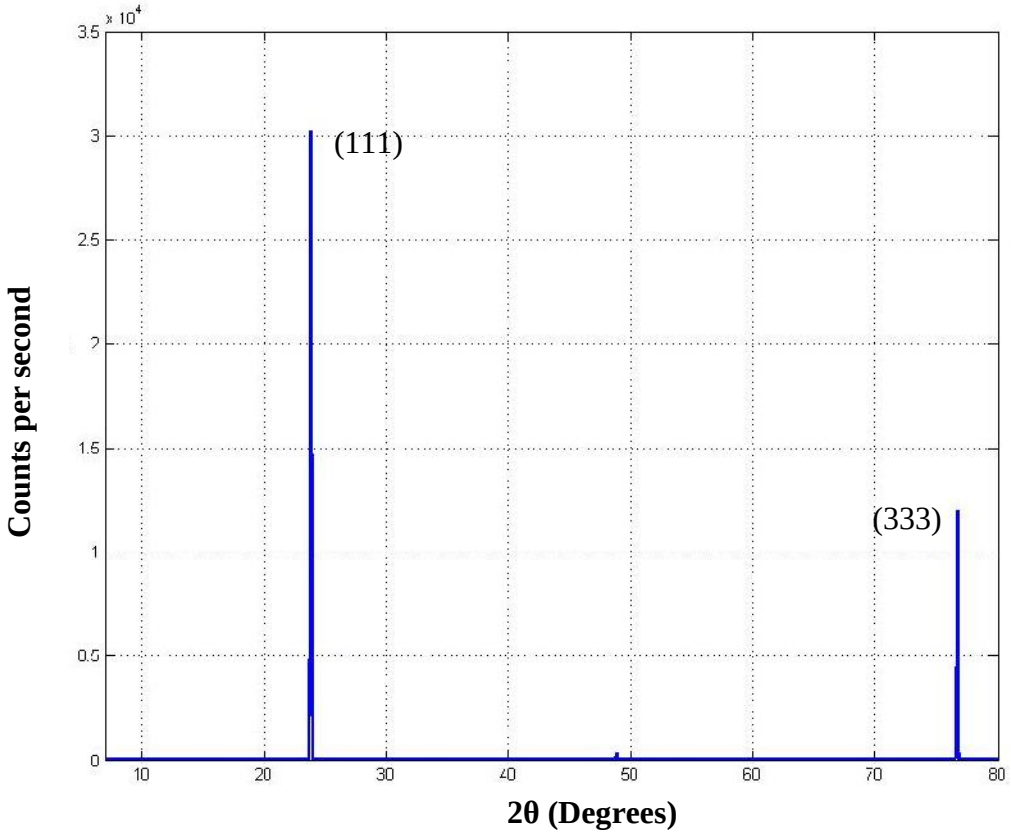

Figure 4.20 A wide 2θ/ω XRD scan on sample 1218

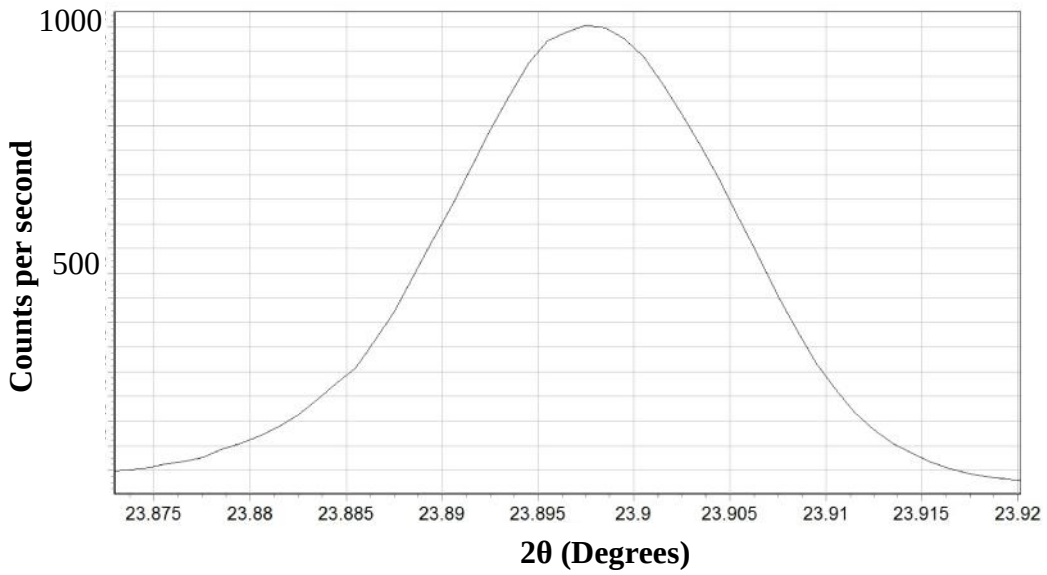

Figure 4.21 A focused 2θ/ω XRD scan on (111) peak of sample 1218

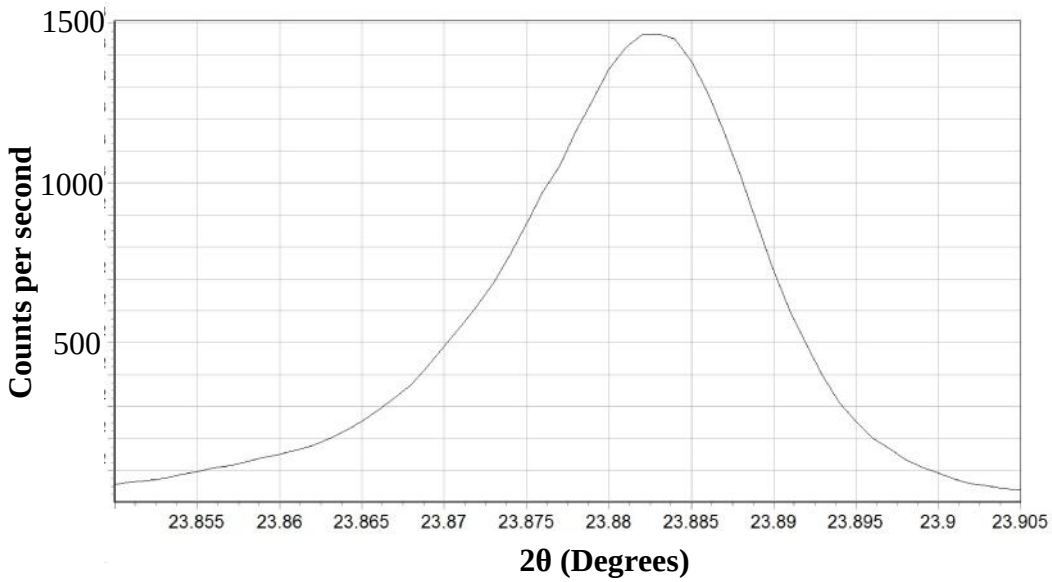

Figure 4.22 A focused 2θ/ω XRD scan on (111) peak of sample 1527

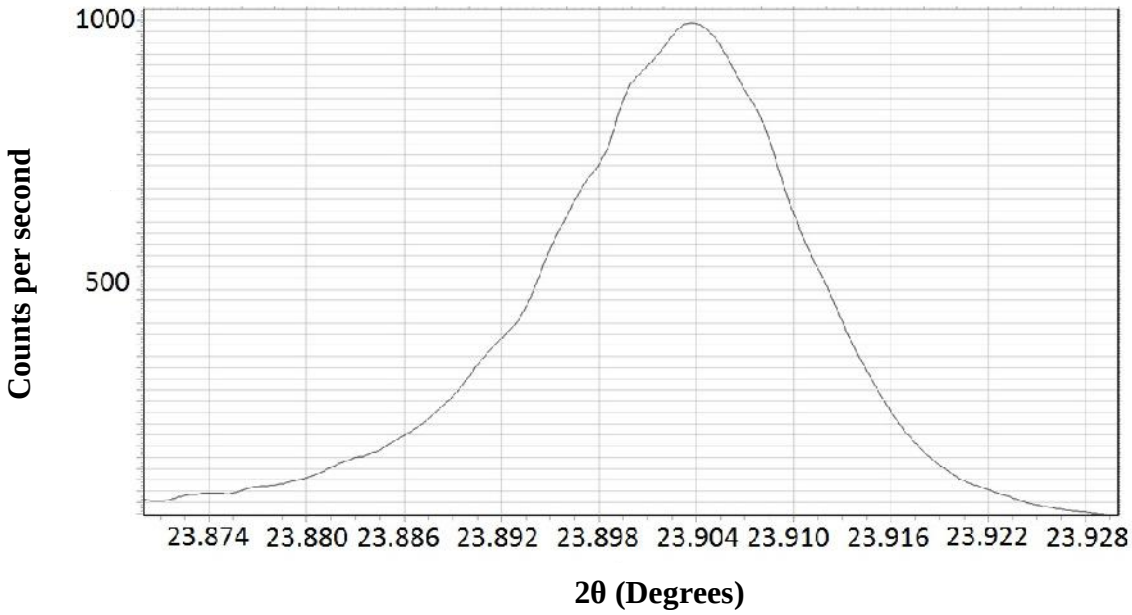

Figure 4.23 A focused 2θ/ω XRD scan on (111) peak of sample 2964

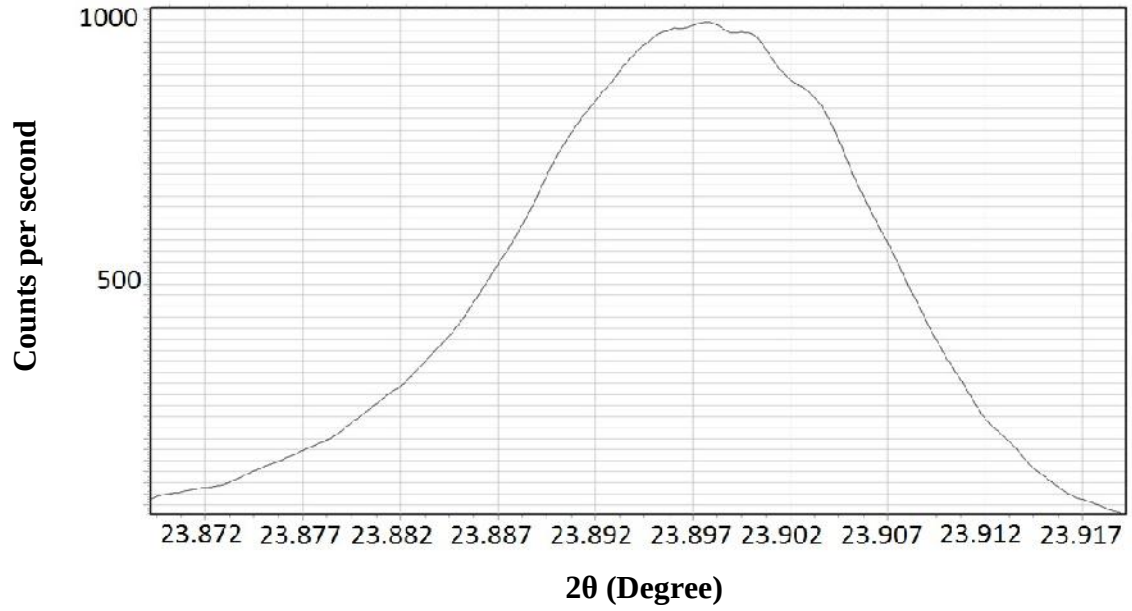

Figure 4.24 A focused 2θ/ω XRD scan on (111) peak of sample 3495

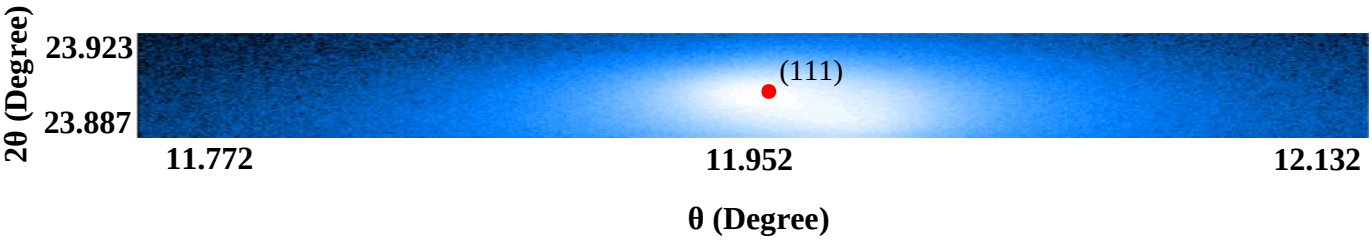

Figure 4.25 Reciprocal space map of the (111) peak for sample 1527

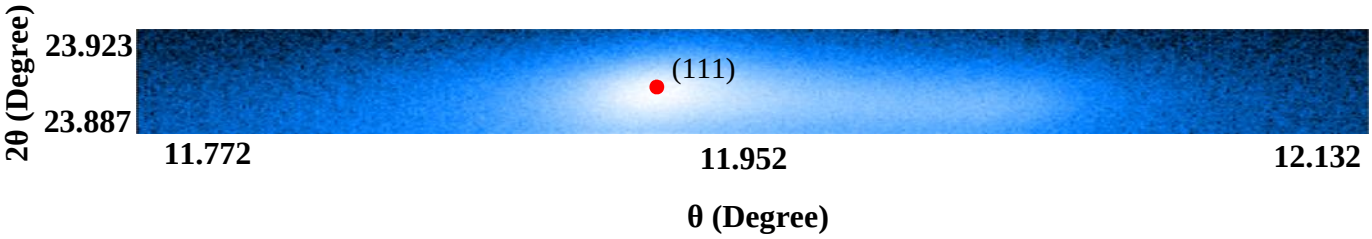

Figure 4.26 Reciprocal space map of the (111) peak for sample 3495

The first peak is the (111) peak and it is studied mainly for our purposes. The reciprocal mapping of the samples 1527 and 3495 shows the (111) peak is broader in 2θ direction for the sample 3495 than the sample 1527 and also there is another peak present in a different ω for the sample 3495 that is not seen in the sample 1527's map. These scans can be used for two different analyses to determine the quality and composition of the sample. The full width at half maximum of the peak is a factor that shows the quality of the sample, as defects and impurities will broaden the peak. The location of the peak provides information about composition and lattice constant of the sample. Table 4.5 shows the location and FWHM of the peak for 2θ/ω scans for different samples, averaged for all scans on different spots.

Table 4.5 Average XRD 2θ/ω scan parameters for all samples

Sample	1218	1527	2964	3495
Average peak location (2θ)	23.8953	23.8893	23.9037	23.8964
Average zinc%	8.83	8.43	9.39	8.91
Average lattice constant	0.64499	0.64515	0.64476	0.64496
Average FWHM	61	60	62.5	76

As XRD parameters show, the lowest FWHM for the XRD peaks is seen for sample 1527. After that samples 1218 and 2964 and the highest FWHM is seen for sample 3495. FWHM of XRD peak is a direct indicator of crystal quality and these results are in agreement with what photoluminescence analyses show. Average zinc concentration of the samples is calculated from the peak location of the peak and the assumption of a linear relation between the peak location and zinc concentration. A linear interpolation between reported XRD peak location for CdTe and ZnTe resulted in the measured zinc concentration in table 4.5. The lattice constants for the samples are also estimated using the location of the peak and Bragg's equation.

For analysing the uniformity of the crystal, we repeated the XRD scans on the same sample for several spots and compared the results. The (111) peak location variations for different samples and the FWHM of each scan are shown in table 4.6. We also performed several scans on the same spot in order to measure the accuracy in the peak location detection, so we can predict an error for the zinc concentration estimation. It results in an error of ±0.06 percent for our prediction of the zinc concentration.

Table 4.6 XRD 2θ/ω scans peaks' location and FWHM range for several scans for all the samples

Sample	1218	1527	2964	3495
Maximum peak shift (degree)	0.0046	0.0104	0.0001	0.0019
FWHM range (arcsecond)	59-63	55-67	62-63	75-77

Photoluminescence and X-ray diffraction correlation

From the analyses that we have done on our data from the temperature dependence photoluminescence to X-ray diffraction, the inhomogeneous broadening factor for the photoluminescence peak, Γ_{inh}, the impurities centers broadening factor for the photoluminescence, Γ_i, exciton-LO phonon coupling constant in the Cody equation and the photoluminescence broadening equation, Γ_{LO} or α, and the FWHM of X-ray diffraction peak are in good agreement. Figure 4.27 and 4.28 show the correlation between the FWHM of X-ray diffraction peak and Γ_{inh} and Γ_i.

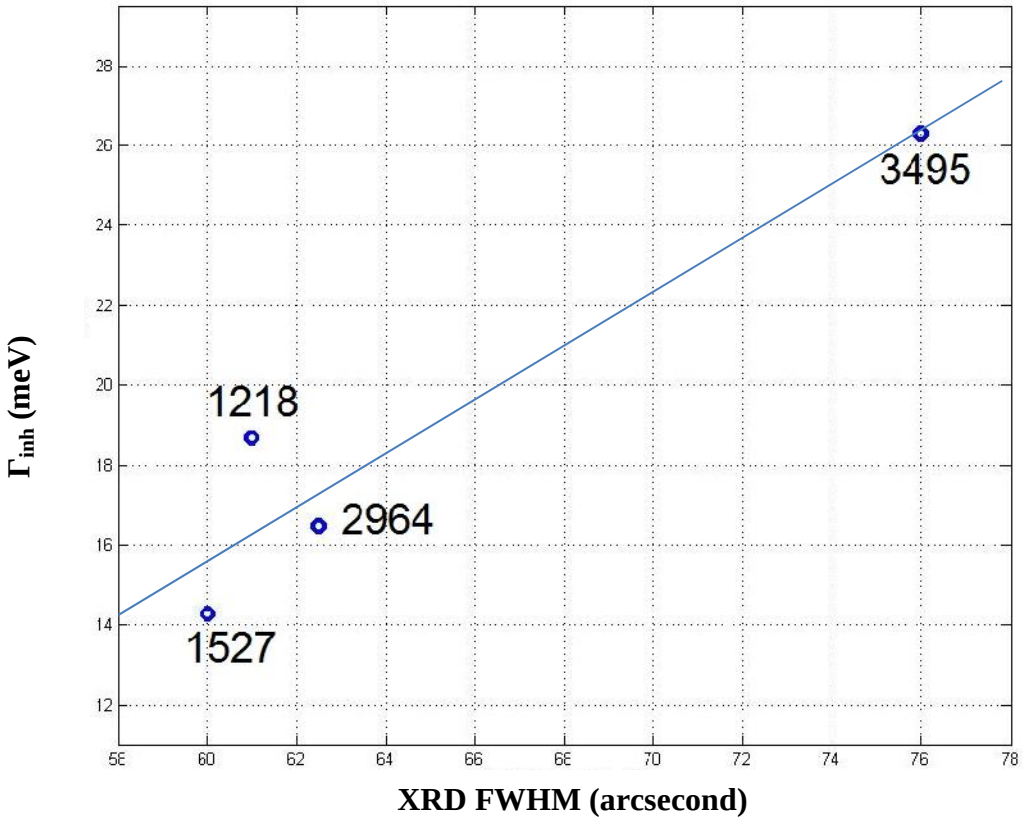

Figure 4.27 Correlation between the FWHM of XRD peak and Γ_{inh}, the inhomogeneous broadening factor for the FWHM of the photoluminescence peak

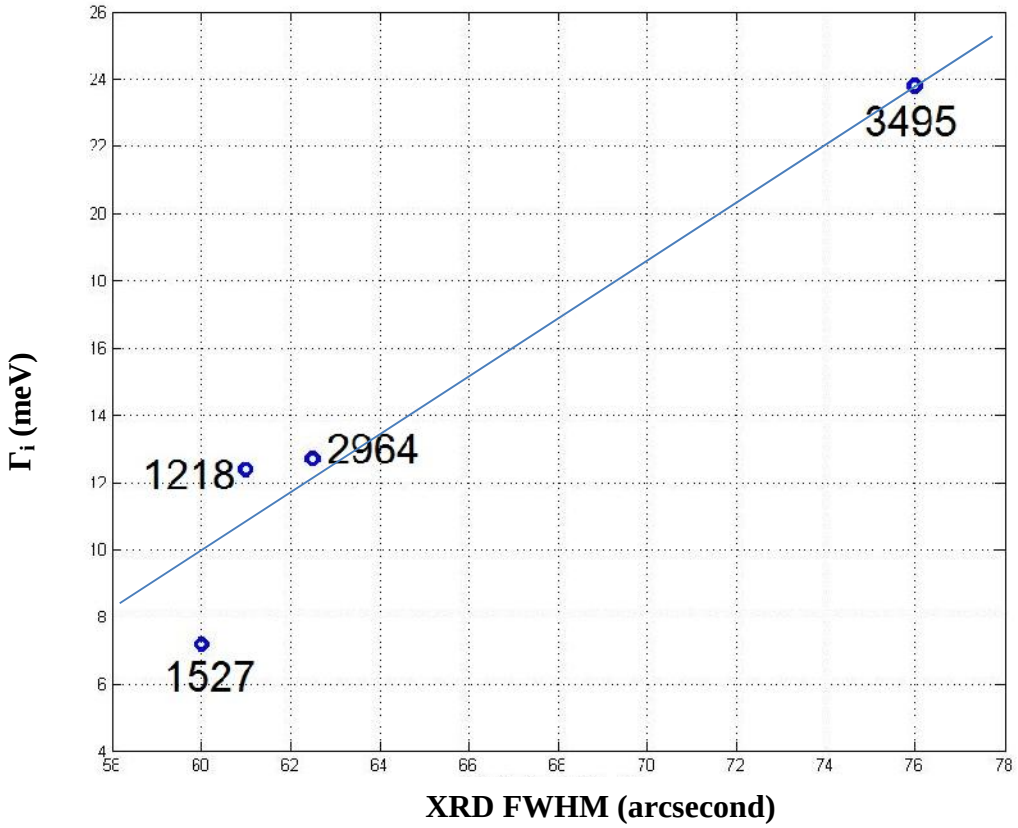

Figure 4.28 Correlation between the FWHM of XRD peak and Γ_i, the impurities centers broadening factor for the FWHM of the photoluminescence peak

The correlation between these data shows that lower concentration of defects, impurities and faults in the crystal structure will result in sharper peak shapes in both X-ray diffraction and photoluminescence. Therefore, the FWHM of the peaks in X-ray diffraction and photoluminescence can be used as an indicating factor of the crystal quality.

5 Conclusion

In this work, four different samples of CZT have been analysed by two different techniques which are both non-destructive. The results have been analyzed from several perspectives and different structural and quality parameters for each sample have been determined. Results from photoluminescence analyses and X-ray diffraction analyses were both in agreement with each other and shows that these techniques can be used jointly in order to provide a comprehensive estimation of different features in grown CZT crystals under different conditions.

From the photoluminescence spectra of the samples, the temperature dependence of the band gap energy has been studied using suggested formulas from several sources. Also, the zinc molar concentration of the samples has been estimated using the band gap energy at low temperatures using several suggested formulas reported for CdZnTe crystals in the literature. Full width at half maximum of the main peak in the photoluminescence spectra is reported to be a direct factor of quality and physical features of the crystal. Several aspects of the factors that affect FWHM of the peak have been studied and physical parameters of this process have been estimated using suggested formulas for fitting the data. Finally, thermal quenching of the photoluminescence peak has been analysed and different processes that result in the observed pattern of peak intensity changes have been determined.

From the X-ray diffraction of the samples, zinc molar concentrations of samples have been estimated and the results were compared with estimations from the band gap energy

in photoluminescence spectroscopy. Moreover, the average lattice constant of the samples has been estimated using the location of peak in X-ray diffraction of each sample. FWHM of X-ray diffraction peak has been analysed as well, as it is related to the quality and uniformity of the sample directly. These results were compared with the analyses of quality and homogeneity resulted from photoluminescence spectroscopy, and a good agreement between these results has been observed.

A correlation was found between the X-ray diffraction linewidth and the low temperature photoluminescence linewidth presumably associated with structural disorder in the crystal. Increased XRD linewidth is associated with a broader PL linewidth for the four different samples that were studied. Although the thermal quenching of the photoluminescence peak intensity gave us a good insight of the different energy levels present in the crystal, no obvious correlation between these data and the X-ray diffraction analyses was found.

In this work, we evaluated the potential of the high resolution XRD and the photoluminescence spectroscopy as methods for characterizing the crystal purity and structural order. These methods have the advantage of being non-destructive. Although we were not able to correlate the crystal properties with the growth conditions, we found that the photoluminescence provided rather detailed information about atomic scale defects and the high resolution x-ray diffraction was sensitive to small changes in structural order which was correlated with the information on defects obtained from PL. Because the photoluminescence and XRD are correlated, the XRD by itself is an

indicator of the density of defects, whenever performing both of these techniques is not possible.

Bibliography

[1] J. F. Butler, C. L. Lingren, and F. P. Doty, "$Cd_{1-x}Zn_xTe$ gamma ray detectors," *IEEE Transactions on Nuclear Science*, vol. 39, no. 4, pp. 605–609, Aug. 1992.

[2] F. P. Doty, J. F. Butler, J. F. Schetzina, and K. A. Bowers, "Properties of CdZnTe crystals grown by a high pressure Bridgman method," *Journal of Vacuum Science & Technology B*, vol. 10, no. 4, pp. 1418–1422, Jul. 1992.

[3] L. Lun, A. Yeckel, J. J. Derby, and P. Daoutidis, "Control of interface shape of cadmium zinc telluride grown via an electrodynamic gradient freeze furnace," in *Mediterranean Conference on Control Automation, 2007. MED '07*, 2007, pp. 1–6.

[4] J. S. Wen, Z. J. Xu, G. Y. Xu, M. Hücker, J. M. Tranquada, and G. D. Gu, "Large Bi-2212 single crystal growth by the floating-zone technique," *Journal of Crystal Growth*, vol. 310, no. 7–9, pp. 1401–1404, Apr. 2008.

[5] S. A. Awadalla, A. W. Hunt, R. B. Tjossem, K. G. Lynn, C. Szeles, and M. Bliss, "Evidence for dislocations or related defects present in CdTe and $Cd_{1-x}Zn_xTe$ crystals," 2001, vol. 4507, pp. 264–272.

[6] K. Zanio, *SEMICONDUCTORS & SEMIMETALS*. Academic Press, 1978.

[7] S. Sen, W. H. Konkel, S. J. Tighe, L. G. Bland, S. R. Sharma, and R. E. Taylor, "Crystal growth of large-area single-crystal CdTe and CdZnTe by the computer-controlled vertical modified-Bridgman process," *Journal of Crystal Growth*, vol. 86, no. 1–4, pp. 111–117, Jan. 1990.

[8] D. J. Olego, J. P. Faurie, S. Sivananthan, and P. M. Raccah, "Optoelectronic properties of $Cd_{1-x}Zn_xTe$ films grown by molecular beam epitaxy on GaAs substrates," *Applied Physics Letters*, vol. 47, no. 11, pp. 1172–1174, Dec. 1985.

[9] K. Oettinger, D. M. Hofmann, A. L. Efros, B. K. Meyer, M. Salk, and K. W. Benz, "Excitonic line broadening in bulk grown $Cd_{1-x}Zn_xTe$," *Journal of Applied Physics*, vol. 71, no. 9, pp. 4523–4526, May 1992.

[10] P. Rehak, "Silicon radiation detectors," in *2003 IEEE Nuclear Science Symposium Conference Record*, 2003, vol. 5, pp. 3375–3379 Vol.5.

[11] J. Llacer, "Planar and coaxial high purity germanium radiation detectors," *Nuclear Instruments and Methods*, vol. 98, no. 2, pp. 259–268, Jan. 1972.

[12] G. G. Stokes, "On the Change of Refrangibility of Light," *Philosophical Transactions of the Royal Society of London*, vol. 142, pp. 463–562, Jan. 1852.

[13] P. J. Dean, "Photoluminescence as a diagnostic of semiconductors," *Progress in Crystal Growth and Characterization*, vol. 5, no. 1–2, pp. 89–174, 1982.

[14] J. Franc, P. Hlídek, P. Moravec, E. Belas, P. Höschl, L. Turjanska, and R. Varghová, "Determination of energy gap in $Cd_{1-x}Zn_xTe$ (x = 0-0.06)," *Semicond. Sci. Technol.*, vol. 15, no. 6, p. 561, Jun. 2000.

[15] E. Cohen, R. A. Street, and A. Muranevich, "Bound excitons and resonant Raman scattering in $Cd_xZn_{1-x}Te$ ($0.9 \leq x \leq 1$)," *Phys. Rev. B*, vol. 28, no. 12, pp. 7115–7124, Dec. 1983.

[16] S. G. Elkomoss, “Excitons Bound to Ionized Impurities: Calculation of the Binding Energies of Exciton—Ionized-Donor Complexes,” *Phys. Rev. B*, vol. 4, no. 10, pp. 3411–3424, Nov. 1971.
[17] R. R. Sharma and S. Rodriguez, “Theory of Excitons Bound to Ionized Impurities in Semiconductors,” *Phys. Rev.*, vol. 153, no. 3, pp. 823–827, Jan. 1967.
[18] D. G. Thomas, J. J. Hopfield, and W. M. Augustyniak, “Kinetics of Radiative Recombination at Randomly Distributed Donors and Acceptors,” *Phys. Rev.*, vol. 140, no. 1A, pp. A202–A220, Oct. 1965.
[19] C. Szeles, “Advances in the crystal growth and device fabrication technology of CdZnTe room temperature radiation detectors,” *IEEE Transactions on Nuclear Science*, vol. 51, no. 3, pp. 1242–1249, Jun. 2004.
[20] S. Jain, “Photoluminscence study of Cadmium Zinc Telluride,” West Virginia, 2001.
[21] K. E. Van Holde, W. C. Johnson, and P. S. Ho, *Principles of physical biochemistry*. Upper Saddle River, N.J.: Pearson/Prentice Hall, 2006.
[22] T. Wang, W. Jie, D. Zeng, G. Yang, Y. Xu, W. Liu, and J. Zhang, “Temperature dependence of photoluminescence properties of In-doped cadmium zinc telluride,” *Journal of materials research*, vol. 23, no. 5, pp. 1389–1392, 2008.
[23] L. Worschech, W. Ossau, and G. Landwehr, “Characterization of a strain-inducing defect in CdTe by magnetoluminescence spectroscopy,” *Phys. Rev. B*, vol. 52, no. 19, pp. 13965–13974, Nov. 1995.
[24] Y. F. Chen, C. S. Tsai, Y. H. Chang, Y. M. Chang, T. K. Chen, and Y. M. Pang, “Hydrogen passivation in $Cd_{1-x}Zn_xTe$ studied by photoluminescence,” *Applied Physics Letters*, vol. 58, no. 5, pp. 493–495, Feb. 1991.
[25] J. L. Reno and E. D. Jones, “Determination of the dependence of the band-gap energy on composition for $Cd_{1-x}Zn_xTe$,” *Phys. Rev. B*, vol. 45, no. 3, pp. 1440–1442, Jan. 1992.
[26] S. P. Tobin, J. P. Tower, P. W. Norton, D. Chandler-Horowitz, P. M. Amirtharaj, V. C. Lopes, W. M. Duncan, A. J. Syllaios, C. K. Ard, N. C. Giles, J. Lee, R. Balasubramanian, A. B. Bollong, T. W. Steiner, M. L. W. Thewalt, D. K. Bowen, and B. K. Tanner, “A comparison of techniques for nondestructive composition measurements in CdZnTe substrates,” *JEM*, vol. 24, no. 5, pp. 697–705, May 1995.
[27] P. Capper, *Properties of Narrow Gap Cadmium-based Compounds*. IET, 1994.
[28] Y. P. Varshni, “Temperature dependence of the energy gap in semiconductors,” *Physica*, vol. 34, no. 1, pp. 149–154, 1967.
[29] J. I. Pankove, *SEMICONDUCTORS & SEMIMETALS V21A*. Academic Press, 1984.
[30] Y. Hwang, Y. Um, and H. Park, “Photoluminescence characteristics of $Cd_{1-x}Mn_xTe$ single crystals grown by the vertical Bridgman method,” *Nanoscale Res Lett*, vol. 7, no. 1, p. 36, Jan. 2012.